A Study on Nano-Si/Polyaniline/ Reduced Graphene Oxide Composite as Anode Material for Lithium-Ion Batteries

by

Kai Li

A thesis
presented to the University of Waterloo
in fulfillment of the
thesis requirement for the degree of
Master of Applied Science
in
Chemical Engineering

Waterloo, Ontario, Canada, 2013

AUTHOR'S DECLARATION

I hereby declare that I am the sole author of this thesis. This is a true copy of the thesis, including any required final revisions, as accepted by my examiners.

I understand that my thesis may be made electronically available to the public.

Abstract

Because of its high theoretical specific capacity (4200mAh/g) when fully lithiated and natural abundance (2nd most abundant element on earth) silicon is considered a promising anode candidate for high energy density lithium-ion batteries. However, the dramatic volume changes (up to 400%) that occur during the lithiation/delithiation processes and the relative low electrical conductivity of silicon prevent the implementation of this technology. In this work, a nano-silicon/polyaniline/reduced graphene oxide composite was synthesized *via* a two-step process: *in-situ* polymerization of polyaniline (PANi) in the presence of nano-silicon followed by combination of the prepared n-Si/PANi binary composite with reduced graphene oxide (RGO) to form a n-Si/PANi/RGO composite. Electron microscopy reveals the unique nano-architecture of the n-Si/PANi/RGO composite: silicon nanoparticles are well dispersed within a PANi matrix which in turn is anchored to the surface of RGO sheets. The n-Si/PANi/RGO ternary composite delivered an initial capacity of 3259 mAh/g and 83.5% coulombic efficiency. In addition, it displayed better rate performance and capacity recovery than either nano-Si or n-Si/PANi. Structural and morphological studies combined with AC impedance analysis suggest that the n-Si/PANi/RGO composite has higher electrical conductivity than the other two materials yielding better performance at high current densities. The good rate performance, high initial specific capacity and stable coulombic efficiency of n-Si/PANi/RGO make it a promising anode material for high energy density lithium-ion batteries.

Acknowledgements

I want to express my deepest gratitude to my research supervisor, Professor Pu Chen, for his constant and valuable support and useful advice. This work would have been impossible without his guidance. He gave me the freedom to pursue my own ideas, which certainly helped mature my personality.

I am also thankful to all members from my research group for their encouragement and help. I would like to thank Dr. Denise Gosselink and Dr. Mingqi Li for all the creative conversations and advices on this work. Special thanks go to Yan Zhao and Yong Ding for conducting SEM and TEM analysis for this work.

I would also like to thank the faculty and staff from the Chemical Engineering Department at University of Waterloo for their fast response no matter when I met problems.

At last, I want to say thanks from the depth of heart to my family, especially my parents. A lot of unexpected things happened while I have been away from home, but my parents have always been my solid support. Being away from home is not easy, but I am glad I made it. Without my parents unconditional love and support I could never have made this far.

Table of Contents

List of Figures

List of Tables

Chapter 1 Introduction

1.1 Context and Motivation

The continuous growth of world population and technological advances of the 21st century create an increasing demand on energy sources. Currently, most of these sources are based on fossil fuels, with only a small contribution from sources such as solar, wind, nuclear, hydroelectric power, and fuel cells. This increasing demand on energy has generated substantial exploitation, and consequently depletion, of oil, coal and gas reserves. According to a study carried in 2003 by J.S. Denker [1], based on the world's current annual energy consumption, fossil fuel resources will be exhausted in 50 to 60 years. At this point, development of alternative new energy has become a critical issue to be solved in the near future. In addition to the shortage of energy resources, the environmental impact of burning fossil fuels must also be taken into consideration. High toxic emissions, increased CO_2 levels, global warming and the resulting climatic changes continue to pose serious threat to society. All of these issues have driven research efforts to the development of alternative and renewable energy sources [2].

As a prominent representative for energy storage, rechargeable Lithium-Ion Batteries (LIBs) play an important role in our everyday life. LIBs dominate the market of consumer portable electronics, surpassing technologies such as nickel cadmium and nickel metal hydride batteries. Because of its high energy-to-weight ratio and a slow self-discharge rate, LIBs also get growing popularity in military, aerospace, medical, smart power grid, and transportation applications.

Because electric vehicles (EVs) do not consume natural reserves and have "zero" emission, they are expected to be the next generation of transportation vehicles, substituting the current gasoline powered fleet. However, the energy densities obtained from LIBs designed for EVs applications are far below that afforded by gas Engines. In addition, cost, lifespan and safety issues are key concerns that restrict the application of LIBs in EVs. Therefore, the development of safe and economic LIBs with high capacity, high energy density, and long cycle life remains as a major challenge [3].

Currently, graphite is used as anode material in commercialized LIBs. Graphite possesses a maximum theoretical specific capacity of 372 mAh/g, limiting the development of carbon based high capacity LIBs. Silicon has attracted much attention as a possible candidate for anode material because of its theoretical capacity (4200mAh/g, the highest among all elements that can alloy with lithium) when lithiated to the $Li_{22}Si_5$ phase and natural abundance (2^{nd} most abundant element on earth). However, silicon is not suitable for direct use in LIBs due to its massive volume change (up to 400%) during the lithitation/de-lithiation processes. In an attempt to solve these problems, a nano-Si/polyaniline/Reduced Graphene Oxide composite has been designed. The synthesis of the engineered composite, surface chemistry and electrochemical studies will be presented in the later chapters.

1.2 Thesis Layout

This thesis describes a silicon based nano-architectured composite for LIBs anodes. The composite was designed in an attempt to alleviate volume changes of silicon during the lithitation/de-lithiation processes and to improve the conductivity properties of the anode. Although the development of cathode materials is also beneficial for achieving high energy density lithium ion batteries, this thesis focuses only on anode materials, more specifically, silicon anodes for LIBs. Below is an outline of the topics covered in this thesis.

Chapter 1 is an introduction to the context and motivation for this study.

Chapter 2 contains the literature review on lithium ion battery technology, its basic components and silicon anodes.

Chapter 3 describes the materials, methods and equipment used in this study.

Chapter 4 portrays the findings of this study, with physical, chemical, and electrochemical data of the prepared composites and discussion of the results.

Chapter 5 is the conclusion of this thesis and brings a final evaluation of the morphology study and electrochemical performance of nano-Si/polyaniline/Reduced Graphene Oxide composite. Suggestions for future work are also proposed.

Chapter 2 Literature Review

2.1 Rechargeable batteries

A rechargeable battery, also known as a secondary battery, is an energy storage system in which the electrochemical reactions are reversible. Rechargeable batteries can provide energy to an external circuit by discharging the current generated by a chemical redox reaction. The spent energy can be restored by charging the system using a reverse current. Rechargeable batteries can be manufactured in different shapes and sizes, which ranges from as small as coin cells to megawatt systems that are made for stabilizing electrical distribution networks. Compared to disposable batteries, rechargeable batteries have lower total operating cost and environmental impact. Although they may have higher initial manufacturing and purchasing cost, they can be recharged cheaply and reused for many times, which lowers the total usage cost. Lead-acid batteries, nickel cadmium batteries, nickel metal hydride batteries and lithium ion batteries are typical representatives for rechargeable batteries [4] and their energy densities have been graphed both volumetrically and gravimetrically in Figure 2.1. From the figure, one can clearly conclude that LIBs have one of the highest energy densities among rechargeable batteries. This means that LIBs can store more energy per volume and weight than most rechargeable batteries. They also operate at higher voltages than most technologies (e.g. about 3.7V for LIBs in comparison to 1.2V for Nickel-Metal Hydride (NiMH) and Nickel-Cadmium (NiCd)).

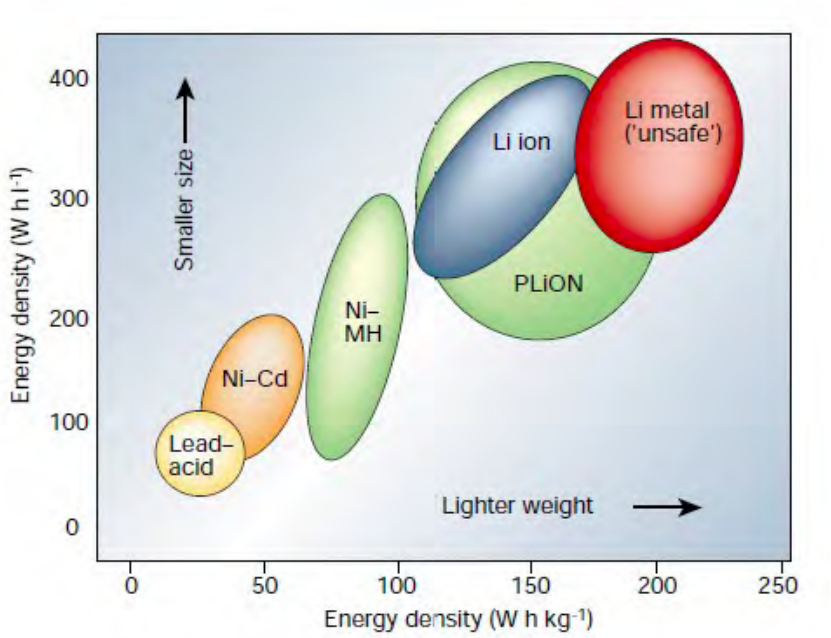

Figure 2.1 Comparison of battery technologies including volumetric energy densities and gravimetric energy densities (Reprinted with permission from Macmillan Publisher Ltd., Issues and challenges facing lithium rechargeable batteries by Tarascon *et al.*, [Nature], copyright 2001) [2]

2.2 Historic background

The use of lithium in a battery system was motivated by the specific intrinsic properties of the element. Lithium is the most electronegative (-3.04V versus the standard hydrogen electrode (SHE)) and the lightest metal in nature (mole weight=6.94g/mol, density= 0.53g/cm3). In principle, these properties could lead to a high energy density lithium based battery system and researchers have not stopped their efforts in this direction [5]. Several primary battery systems using lithium as anode material were proposed one after another in 1970s, such as $Li/(CF)_n$ [6], $Li/SOCl_2$ [7], Li/MnO_2 [8] and $Li/Ag_2V_4O_{11}$ [9], most of which were designed for medical and military purposes. The development of rechargeable lithium batteries came out from the discovery that some special inorganic compounds could react with lithium ions reversibly. At that point, battery systems using titanium sulfite (TiS_2), chalcogenides ($NbSe_3$) and molybdenum sulfite (MoS_3) [10,11] as cathode materials coupled with lithium metal as anode material were developed. The discovery of reversible intercalation compounds opened up a new era for rechargeable lithium batteries. The electrochemical reaction between the intercalation materials and lithium ions occurs reversibly when lithium ion inserts to and extracts from the intercalation

hosts. During the intercalation/de-intercalation processes there are no significant phase changes, leading to small or no damage to the host material structure. However, during the early development stages of rechargeable lithium batteries, many difficulties were encountered. Stable electrolyte, consisting of proper lithium salts in an organic solvent, had to be identified and coupled with reversible cathode materials.

Initially, lithium metal was used as the anode material in rechargeable lithium batteries. However, upon charge/discharge, lithium dendrites gradually grow on the anode, which results in poor cycle performance and eventual short circuit to cells. Moreover, the short circuit may lead to serious safety issues with risk of fire and cell explosion. As a result, LIBs were developed in which both electrodes are made of materials containing lithium ions. In 1977, Samar Basu demonstrated the electrochemical intercalation of lithium ions in graphite, providing an alternative to the lithium metal electrode [13]. In 1979, John Goodenough and K Mizushima [12] built a rechargeable battery system lithium cobalt oxide ($LiCoO_2$) as the cathode material. The innovation of this technology is that $LiCoO_2$ is a stable cathode electrode material and acts as a donor of lithium ions, which means that it can be coupled with various kinds of anode electrode materials other than lithium metal. Since graphitic carbon was found to be dimensionally stable for the lithium insertion and extraction, graphite became the choice as anode material for commercialized LIBs, displacing lithium metal and lithium alloys (which usually involve volume changes in the range of 200-600%). In 1983, Thackeray, Goodenough, and coworkers [14] demonstrated the use of spinel lithium manganese oxide ($LiMn_2O_4$) as a cathode material. Given its low-cost, reasonable electronic and lithium ion conductivity, and good structural stability, $LiMn_2O_4$ is a promising cathode material for LIBs. In 1996, Goodenough, Akshaya Padhi and coworkers demonstrated lithium iron phosphate ($LiFePO_4$) and other phospho-olivines (lithium metal phosphates with the same structure) as cathode materials [15].

The combination of intercalation anode and cathode materials together with an appropriate electrolyte has been a major task in the field of the LIBs. In 1991 Sony Corporation commercialized the first rechargeable LIBs using $LiCoO_2$ as cathode and graphite as anode [119]. The potential of the battery was 3.6V, which is almost 3 times as that of Ni-Cd and NiMH rechargeable batteries. It also provided higher energy density ranging from 120 to 150Wh/Kg,

which is over two times that of Ni-Cd and NiMH technologies. Today, other than serving as a dominant energy sources for consumer electronics, LIBs are also known as playing a more and more pivotal role for applications in military, aerospace, medical, smart power grid and electric vehicles (EVs).

2.3 Principle of operation of lithium-ion batteries

The LIBs were first termed as "rocking chair" batteries by Armand [16], since the lithium ions rock back and forth between cathode electrode and anode electrode. Both anode and cathode electrodes work as hosts for reversible lithium ion insertion and extraction while the electrolyte provides an ionic pathway for lithium ion transport. The schematic diagram of the LIBs is shown in Figure 2.2.

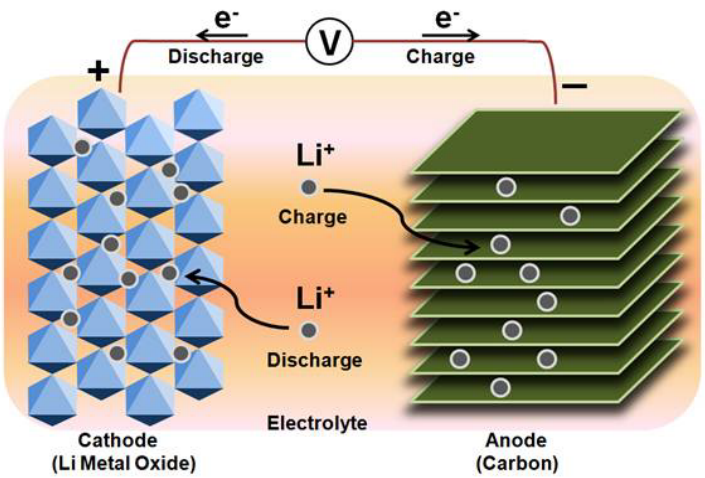

Figure 2.2 Schematic diagram of a conventional Lithium-Ion Batteries (Reprinted with permission from John Wiley and Sons Inc., Nanostructured Silicon Anodes for Lithium Ion Rechargeable Batteries by R. Teki *et al.*, [Small], copyright 2009) [17]

Equations (2-1) and (2-2) represent the reactions occurring on the anode and cathode during the charging process and are reversed upon discharge.

Anode reaction:

$$xLi^+ + 6C + xe^- \leftrightarrow Li_xC_6 \qquad (2\text{-}1)$$

Cathode reaction:

$$LiMn_2O_4 \leftrightarrow xe^- + Li_{(1-x)}Mn_2O_4 + xLi^+ \qquad (2\text{-}2)$$

The energy storage mechanism for LIBs can be explained as following: during the charging process lithium ions are released from the cathode host, travel through the electrolyte and separator and reach the anode. After this, lithium ions are inserted into the anode structure. The reverse process happens during discharge, that is lithium ions are extracted from anode material and inserted into cathode structure. The electrochemical reaction in LIBs follows the Gibbs-Helmholtz equation [4]:

$$\Delta G = \Delta H - T\Delta S \qquad (2.3)$$

Where,

ΔG is free energy for the reaction

ΔH is enthalpy for the reaction

ΔS is entropy for the reaction

The free energy ΔG is also related to the potential difference between cathode electrode and anode electrode based on Faraday's law:

$$\Delta G = -nFE \qquad (2.4)$$

Where,

n is the number of the transferred electrons

F is the Faraday constant

E is the potential difference between the cathode and anode electrodes

Hence, the design of a LIBs system strongly depends on the careful pairing of both working electrodes in order to achieve a high operating voltage.

2.4 Anode materials for lithium-ion batteries

Lithium metal was the anode material initially used in rechargeable lithium batteries. However, lithium deposition on the anode during charge usually leads to the formation of dendrites, which results in poor cycle performance and cell short circuit. Therefore, alternative materials must be used as anode in LIBs. In order to be qualified as a Lithium-Ion Battery anode a material must fulfill some basic requirements [4]:

a) Low electrochemical potential versus lithium: so as to increase the operational voltage of the cell;
b) Large amount of lithium ions that can be accommodated in the material: so as to increase the energy of the cell.
c) Small (ideally none) structural changes or damage of the material during repeated lithium ion insertion/ extraction: so as to guarantee good cycling performance.

In the following sections a survey of the prominent materials used or investigated as anodes in LIBs is presented.

2.4.1 Carbon based anode materials

Currently, graphitic carbon is commercially used as the anode in LIBs. It can be obtained from a variety of carbon sources ranging from natural graphite to polymer resins. Various treatment methods on the carbon sources result in final carbon materials obtaining different properties. In general, the carbon materials used as anodes in LIBs can be divided into graphite, hard carbon and soft carbon.

Graphite has a layered structure that consists of ABAB layers, which are held together by van der Waals force. The intercalation of the lithium ions into the interlayers of the graphite forms LiC_6, which leads to the 372mAh/g theoretical capacity of graphite. The intercalation of lithium ions into graphite and its electrochemical properties has been well studied [18].

Soft carbon is made from organic precursors that form a semi-fluid state when decomposed whereas hard carbon is made from organic precursors that char as they pyrolyze. Table 2.1 shows

the comparisons of carbon anodes. Hard and soft carbon anodes have a wide range of capacity values depending on starting materials and processing conditions (temperature and pressure).

Because of its natural abundance and small volume change upon lithiation, carbon is still considered a good anode material candidate and approaches like particle coating, surface treatment, and nanosizing/nanostructuring are often used to improve its cycling performance. Despite these efforts, carbonaceous anodes suffer from short cycle life or large irreversible capacity in the first cycle. In addition, its low specific capacity limits its application in large energy storage systems. Increasing the specific capacity while maintaining a good cycle life is the main challenge for making a good carbon based anode material for future LIBs.

Table 2.1 Comparison of the properties of different carbon materials in LIBs [19]

Material	Initial Capacity (mAh/g)	Reversible capacity (mAh/g)	First Cycle efficiency (%)
Graphite	372	342	92
Soft carbon	275	235	85
Hard carbon	480	370	77

2.4.2 Alloy based anode materials

Many metals can react with large amounts of lithium and form Li_xM_y alloys, which could be applied as lithium ion battery anodes. These metals include Si, Sn, Sb, Al, Mg, Bi, In, Zn, Pb, Ag, Pt, Au, Cd, As, Ga, Ge, etc. Because of the high cost of some of these metals, only some of them have been well studied. Table 2.2 shows a comparison of the properties of various metals used as anodes for LIBs. Despite their potentially high specific capacity, these alloys experience a tremendous volume change when reacting with lithium, which results in material and electrode cracking and eventually failure. In order to alleviate the dramatic effects of the volume changes, these materials have been synthesized in nanosized structures resulting in much improved cycling performance [20]. Besides reducing particle size of the metals, other solutions to lighten the volume change were also proposed: a) incorporating ductile Li-ion conducting metals or polymer matrix with Li-alloys [21]; b) embedding the alloys within matrix which could partially hold the volume change [22].

Table 2.2 Comparison of various metals used as anodes for Lithium-Ion Batteries [25]

Materials	Si	Sn	Sb	Al	Mg	Bi
Density (g/cm3)	2.33	7.29	6.7	2.7	1.3	9.78
Lithiated Phase	$Li_{22}Si_5$	$Li_{22}Sn_5$	Li_3Sb	LiAl	Li_3Mg	Li_3Bi
Theoretical Specific Capacity (mAh/g)	4200	994	660	993	3350	385
Volume Change (%)	420	260	260	96	100	215
Potential vs. Li (V)	0.4	0.6	0.9	0.3	0.1	0.8

Intermetallic compounds have been extensively studied as anode materials for LIBs. They are formed by one active component, which alloys lithium, plus another inactive metal(s) that will be displaced by lithium, creating a matrix where the lithiated alloy can be absorbed. The inactive matrix must be conductive and mechanically ductile so as to bring structural stability to the intermetallic electrode and alleviate the volume change of the active component when alloying. For example, Ou Mao and colleagues [23] obtained $FeSn_2$ alloy by high-energy ball milling, which was used as anode material for LIBs and showed better cycling performance than pure Sn. The intermetallic alloys can be any binary, ternary or even multi-element combination of inactive/active (to lithium) components.

The other solution is embedding the alloys in a conductive polymer matrix. In this case, the conductive polymer acts as "bridges" connecting the alloys particles together and providing a better pathway for electrons. Furthermore, the elasticity of polymer matrix also helps holding the large volume change during alloying/de-alloying process. For instance, Jie-Jian Cai and co-workers [24] embedded silicon nanoparticles in a conductive polyaniline matrix. The composite showed better cycling and rate performance than pure nano silicon. With the aid of synthetic organic chemistry, several new conductive polymers have been successfully synthesized in recent years. However, a lot of work is still necessary to design and synthesize new polymers with good conductivity and elasticity that could be applied as matrices for lithium alloys [54].

2.4.3 Metal oxide anode materials

Metal oxide anode materials can be generally classified into two categories. One is the insertion compounds: metal oxides able to intercalate lithium ions at low potential. The other group of metal oxides uptakes lithium by a disproportionation mechanism which usually produces the reduced metal oxide captured in a matrix of Li_2O [120].

2.4.3.1 Insertion metal oxides

$Li_4Ti_5O_{12}$ is one of the representatives for insertion metal oxide anodes. It was first identified by Ohzuku and colleagues [28] as a zero-strain insertion material with excellent cyclability in 1995. The relatively high insertion potential *versus* Li makes $Li_4Ti_5O_{12}$ electrode safer than graphite. The lithium intercalation/de-intercalation process in $Li_4Ti_5O_{12}$ can be represented as follows:

$$Li_4Ti_5O_{12}+3Li \leftrightarrow Li_7Ti_5O_{12} \qquad (2.5)$$

This reversible electrochemical reaction is accompanied by very little change in lattice dimensions, which makes $Li_4Ti_5O_{12}$ an almost 'zero strain' electrode material with good cyclability and only small capacity fade upon cycling. The major drawbacks of the $Li_4Ti_5O_{12}$ are:

a) The theoretical specific capacity of $Li_4Ti_5O_{12}$ is 172mAh/g, which is much lower than other metal oxides; it is only about half of the capacity of graphite and 1/3 of that of SnO_2.
b) The intrinsic conductivity of $Li_4Ti_5O_{12}$ is 10^{-9} S/cm, which is over 10 orders of magnitude lower than that of graphite. Therefore, $Li_4Ti_5O_{12}$ displays severe concentration polarization when cycled at high currents, which results in poor rate performance.
c) The tap density of $Li_4Ti_5O_{12}$ powder is relative low, resulting in low volumetric capacity, which in turn is detrimental for the battery energy performance.

Considering that $Li_4Ti_5O_{12}$ have no side reactions with electrolytes directly leading to irreversible capacity, researchers have nanostructured the material to improve Li intercalation properties by increasing electrode/electrolyte interfacial contact area and improving charge transport. Kavan and Grätzel [29] synthesized $Li_4Ti_5O_{12}$ spinel nanowires which delivered a first discharge capacity of 165mAh/g at a 1/10 C rate and 93% capacity retention at 10 C rate. In addition, recent research results showed that doping and carbon coating of $Li_4Ti_5O_{12}$ could improve materialist electrical conductivity and improve cycling performance [30].

2.4.3.2 Reduction/alloying metal oxide

This type of metal oxides has been studied intensively [4, 26]. Upon lithiation, a two-step reaction usually occurs: the metal oxide first react irreversibly with lithium, which leads to the formation of metal/suboxide particles dispersed in a Li_2O matrix. This process creates a favorable environment that facilitates the subsequent reversible lithium alloying/de-alloying step: the lithia matrix offers free volume to accommodate the mechanical stresses associated with the alloying/de-alloying process [4].

Tin oxides, such as SnO, SnO_2 and Li_2SnO_3, are typical examples from this category and they can deliver gravimetric capacities of over 600mAh/g. The major problem with tin oxide anodes is the large irreversible capacity in the first cycle (up to 40%), which usually comes from the Li_2O formation. To compensate this irreversible capacity, cells need to be assembled with excess cathode material. However, by creating a nanosized tin oxide structures, the above-mentioned problem could be alleviated. L. Yuan and colleagues [27] improved the electrochemical performance of the SnO_2 and increased the coulomb efficiency by creating a spherical porous nanostructure *via* the spray pyrolysis technique. The pores between nanosized particles reduce the aggregation of Sn particles while acting as a buffer which accommodates the volume change of Li-Sn alloying/de-alloying process.

2.5 Silicon anode materials

Silicon has attracted lots of attention because its high theoretical capacity (4200mAh/g, when fully lithiated to $Li_{22}Si_5$) and natural abundance (2^{nd} most abundant element on earth). When alloying with lithium, Si can form several different alloys, such as $Li_{12}Si_7$, $Li_{14}Si_6$, $Li_{13}Si_4$, $Li_{15}Si_4$, $Li_{22}Si_5$, etc. For the lithium richest phase, the alloying reaction is represented as:

$$22Li^+ + 5Si + 22e^- \leftrightarrow Li_{22}Si_5 \qquad (2\text{-}6)$$

Successful application of silicon anodes in Lithium-Ion Batteries could provide over 10 times increase in specific capacity for anode in comparison to the commercialized systems available today. When paired with conventional cathode and electrolyte, the total capacity could be doubled or even tripled. However, the dramatic volume changes (up to 400%), which occurs during lithiation/de-lithiation processes, still prevent the realization of this technology.

The structural variations in the silicon anodes particles have three serious repercussions [25]:

a) Anode material pulverization. The massive volume change during lithiation/de-lithiation process generates large stresses within the silicon particles. This leads to creation and propagation of cracks and pulverization of the silicon anodes, with subsequent loss of electrical contacts between silicon particles, which causes capacity loss. This mechanism could explain the capacity fading for most of the silicon anodes.

b) Morphology and volume change of whole Si electrode. The volume changes and loss of contact between the silicon particles affect the morphology of the entire electrode and ultimately makes the electrode material to peel-off from the current collector, resulting in failure of the cell. This problem adds another layer of challenge to the full cell design.

c) Instability and irregularity of the solid-electrolyte interphase (SEI). When the anode potential is lower than 1V versus Li/Li^+, the organic electrolyte decomposes at the surface of the electrode particles. Since the potential for alloying between lithium and silicon is 0.4V versus Li/Li^+, electrolyte decomposition is a thermodynamically favored process on the silicon anode. The decomposition products deposit as a layer on the surface of silicon anode, forming what is known as "solid-electrolyte interphase" (SEI). In order to achieve a LIB with good cyclability, a stable and continuous SEI layer is considered critical. The SEI should also be ionically conductive to allow lithium ions transport through it, while electronically insulating so as to prevent further side chemical reactions. However, because the silicon surface is more reactive towards electrolytes than graphite, a complex SEI composition that includes hydrocarbons, $C_2H_5OCOOLi$, $LiCO_3$, Li_2O, LiF, and silicon-containing products (such as lithium silicates, SiF62-, etc.) emerges [31]. Additionally, because of the expansion and contractions of the silicon particles, the SEI is broken upon cycling. The re-exposure of the fresh Si surface to the electrolyte brings continuous changes to SEI, both in thickness and composition.

The schematic diagram in Figure 2.3 shows the three Si electrode failure mechanisms.

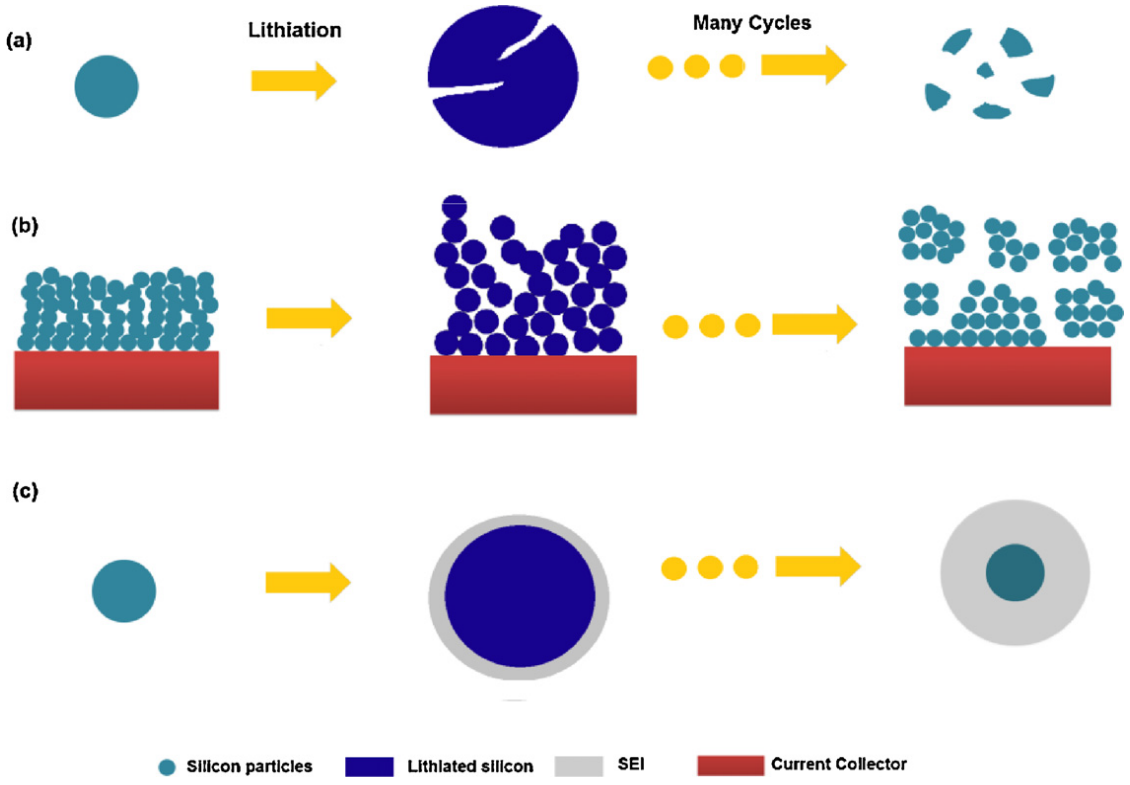

Figure 2.3 Si electrode failure mechanisms: (a) Anode material pulverization. (b) Morphology and volume change of whole Si electrode. (c) Continuous change of solid-electrolyte interphase (Reprinted with permission from Nature Publishing Group, Designing nanostructured Si anodes for high-energy lithium ion batteries by Hui Wu, Yi Cui, [Nano Today], copyright 2012) [25]

Many attempts have been made in order to overcome the volume change issue that prevents the practical application of silicon anodes in LIBs. Graetz and colleagues [32] suggested that the critical silicon particle size should be lower than 300nm to prevent cracking. The authors achieved this critical value using the theory of crack propagation (2-7)

$$\alpha_c = \frac{2k_{1c}^2}{\pi\sigma^2} \qquad (2\text{-}7)$$

Where,

α_c is the critical size for crack propagation, in m;

k_{1c} is the fracture toughness, in MPa/m$^{1/2}$;

σ is the yield strength, in GPa.

By substituting k_{Ic} as 0.751 MPa/m$^{1/2}$ and σ as 1.1GPa for silicon particles, the critical particle size of 300nm is obtained. Studies on nano and bulk silicon anodes were extensively carried out afterwards to verify and study the basics behind the assumption, many results from which turned out to be matching with the assumption [33-34]. Hong Guo and colleagues [33] fabricated silicon thin film on copper foil by using radio-frequency magnetron sputtering. Films with thickness around 300nm delivered a reversible specific capacity of 3500mAh/g and retention of 90% after 25 cycles.

The electrochemical performance of a pure silicon anode with an average particle size of 10μm has also been studied [34]. Figure 2.4 displays the charge/discharge profile for this material, which shows high irreversible capacity for the first-cycle (around 2650mAh/g) and very low coulombic efficiency (about 25%). The specific capacity fades very quickly during the following repeated cycles with only about 30% capacity retention after 5 cycles. This is common behavior in microscopic silicon powder anodes. Ji Heon Ryu and colleagues pointed out that large volume changes and poor electrical conductivity of silicon account for the poor cyclability of this anode material. The authors proposed two approaches to solve these two problems, namely: a) use elastomeric polymer binder, which could help restore the contact area between Si and carbon particles even after a repeated volume changes; b) use of Si composite materials or surface-coated Si with highly conductive carbon, ceramic or metal which could increase the electrical conductivity of the silicon powder anodes and also help curb the large volume changes [34].

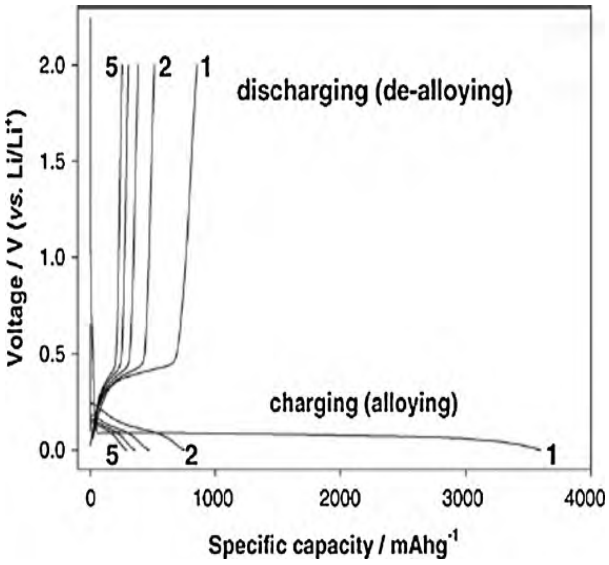

Figure 2.4 Charge–discharge voltage profiles of a pure silicon anode with an average particle size of 10μm (Reprinted with permission from Electrochemical Society, Failure Modes of Silicon Powder Negative Electrode in Lithium Secondary Batteries by Ji Heon Ryu *et al.*, [Electrochemical and Solid-State Letters], copyright 2004) [34]

In general, silicon anodes for LIBs could be divided into two categories: silicon composites and silicon only materials (usually come with structural differences) [3].

2.5.1 Silicon composite anodes for Lithium-Ion Batteries

Silicon composites for LIBs are usually a combination of silicon with one of carbon-based materials, lithium active/inactive elements, or resilient polymer matrix.

2.5.1.1 Composites of silicon with carbon and carbon derivatives

Addition of carbon additives or carbon coatings on silicon anode materials can provide electrical connection between silicon particles and the entire anode. There are numerous ways to prepare the Si/C composites, such as ball milling silicon particles with different carbon materials, synthesis of silicon dioxide on carbon-based materials followed by reduction of the oxide, thermal and chemical vapor deposition techniques, pyrolysis of silicon-carbon precursors, etc.

Guo and colleagues [35] synthesized a Si/C composite by high-energy ball-milling silicon and polypyrrole followed by pyrolysis of polypyrrole to carbon. The composite with roughly 10% silicon content showed a stable reversible specific capacity of around 1000 mAh/g. Zhang and

colleagues [36] ball milled silicon particles with carbon nanotubes, establishing a special matrix with lamellar structure; the resulting composite showed an initial capacity around 1500 mAh/g and a reversible capacity of 584 mAh/g after 20 cycles.

By magnesiothermically reduction of diatomaceous earth, Lanyao Shen and associates [37] created a three-dimensional porous structured silicon anode. After treatment with HCl the product had a porous structure with average pore size around 200nm, similar to that of the diatomaceous earth. The final product showed an initial discharge capacity of 1818 mAh/g, retaining 633 mAh/g after 30 cycles.

Thermal and chemical vapor deposition techniques have also been used for preparation of silicon/carbon composites [38]. Yoshio and co-workers [39] synthesized silicon particles coated with carbon by thermal vapor deposition (TVD). The composite maintained a high reversible capacity of 800 mAh/g for over 20 cycles. S. Iaconetti and colleagues [40] used chemical vapor deposition (CVD) to deposit carbon on a milled mixture of silicon and diluent carbons with an organic gas as precursor. The composite showed a stable reversible 500mAh/g for more than 30 cycles.

Lu Yue and colleagues [41] polymerized 3,4-ethylenedioxythiophene (EDOT) in an aqueous solution of nano-silicon and poly (styrene sulfonate) (PSS) and obtained Si/PEDOT:PSS, which was subsequently carbonized to form a composite of nano-silicon embedded in amorphous carbon. The material exhibited good electrochemical performance, retaining a specific capacity of 768 mAh/g and coloumbic efficiency of 99.2% after 80 cycles only with a very small capacity loss (~ 2.80%) for the first cycle and 0.48% per cycle overall capacity fading. A Si-carbon composite with silicon and graphite embedded in carbon matrix which was pyrolyzed from petroleum pitch demonstrated reversible capacity close to 700 mAh/g for over 50 cycles when used as anode material in LIB [42].

Graphene also have been extensively studied in silicon composites [43-44]. Graphene is a one-atom-thick two-dimensional material, which could provide superior electrical conductivity, high surface area, and excellent thermal and mechanical properties. Graphene/ nano-silicon composites with improved cycle performance have been reported [43]. The composite with graphene sheets

made from thermally expanded graphite exhibits an excellent cycling performance accompanied with a high initial capacity of 2750mAh/g and about 83% capacity retention after 30 cycles. Zhou and colleagues [44] successfully inserted nano-silicon particles into graphene sheets by a novel method combining freeze-drying and thermal reduction. The nano-Si/graphene composite exhibited enhanced cycling and rate performances when compared to pure nano-Si particles.

2.5.1.2 Composites of silicon with lithium active/inactive matrices

Composites of silicon with active matrix

In this subcategory, both the silicon and the host matrix react with lithium to form alloys. The strategy is to have one component alloying with lithium while the other acts as a buffer to alleviate the volume changes, since the two reactions have different onset potentials. SiSn and Mg_2Si alloys are two typical examples for this kind of composites.

Xiao and colleagues [45] reported a unique nanostructure, produced by phase separation of Si and Sn in a thin film, which could mitigate the mechanical degradation effects by preventing the generation and propagation of micro-cracks within the electrodes during the lithiation/de-lithiation processes. The composite with an optimum Si/Sn ratio ($Si_{54}Sn_{46}$), where amorphous Si nanoparticles were embedded in the Sn matrix, showed an excellent cycling performance with a specific capacity around 1400 mAh/g for over 25 cycles.

Mechanically activated annealing (MAA) of Mg and Si followed by ball milling with carbonaceous materials such as carbon nanotubes (CNTs) and carbonaceous mesophase spheres CMS in different ratios was carried out by J.M. Yan *et al.* [46] to synthesize Mg_2Si/C composites. The best composites delivered reversible capacities at 400 mAh/g with reasonable cyclic performance. The authors suggested that the enhanced performance stems from a lower charge-transfer resistance, a stable reactive interface, and reduced volume expansion.

Despite offering some improvement in terms of conductivity and initial capacity, the lithium-active silicon composite anodes usually have low reversibility during repeated charge/discharge and shorter cycle life than that of mixed active/inactive composites [46-47].

Composites of silicon with inactive matrices

This type of silicon composite anodes consists of silicon particles embedded in an electrochemically inert matrix which serves to minimize the effect of volume changes. The matrix could be metals such as Co, Fe, Ni and Ca [48], metal oxides such as Al_2O_3 [49] and Li_2O [50], or ceramics such as TiN [51], Si_3N_4 [52] and SiC. Significant loss in reversible capacity is usually observed with addition of these inactive materials.

G.X. Wang and colleagues [47] successfully synthesized nanocrystalline NiSi alloy powders *via* high energy ball-milling. The composite exhibited a high initial specific capacity of 1180 mAh/g with significant capacity fading in the following cycles. Heon-Young Lee and co-workers [53] prepared a carbon-coated nano-Si dispersed oxides/graphite composite by mechanochemical reduction of SiO by Al with the help of ball-milling followed by pyrolysis of coal–tar pitch with nano-Si dispersed oxides/graphite in argon flow. The composites showed good cycling performance with an acceptable irreversible capacity on the first cycle, which was attributed to the combination the uniform distribution of nano-sized Si, an enhanced electronic and ionic conduction by carbon coating and the buffering action of graphite. Similarly, Liu and colleagues [50] created a novel silicon composite by dispersing nanosized silicon within porous, elastic and conductive oxide/carbon matrix. The composite was prepared *via* a mechanochemical reduction of SiO under ball milling, followed by the pyrolysis of poly (vinyl chloride)–co-vinyl acetate. It showed a stable capacity of 620mAh/g for up to 100 cycles without significant capacity fading.

X.N. Zhang *et al.* [52] prepared Si–Si_3N_{4p} (amorphous Si_3N_4 nanoparticles) and Si–Si_3N_{4w} (α-Si_3N_4 whiskers) composites with different silicon contents *via* ball milling. The inactive components (Si_3N_{4p} and Si_3N_{4w}) in the composites acted as a buffer matrix to support and prevent the aggregation of silicon particles during cycling. The composites with Si_3N_{4p} had larger reversible capacities and better cycle performance. A reversible capacity of 470 mA h/g was obtained for the Si–Si_3N_{4p} composite containing 30 wt.% Si.

One possible disadvantage of the inactive components is that they may slow down or even block lithium diffusion and electron transfer to silicon, which may lead to low capacity. In order to avoid this potential problem, the selection for inactive components should follow two requisites:

a) Good ionic and electrical conductivities;

b) Good mechanical strength.

In terms of mechanical strength, research shows that inactive components matrix with high yield strength, low ductility, and low elastic modulus provide better volume compensation during cycling. This means that the matrix must have a large elastic modulus and a good tolerance to stress when the active particles expand so that the inactive particles are under high compressive residual stress during Li insertion. Further studies are required on this topic [54].

2.5.1.3 Composites of silicon with resilient polymer matrix

Carbon coatings with high electronic conductivity can buffer the large volume changes during the lithiation/de-lithiation process and also provide well dispersion of silicon particles, which helps prevent agglomeration. A conductive polymer matrix (e.g. polyporrole or polyaniline), in which Si is embedded, could be used as such matrix. These polymers are very stable in the voltage window of 0.00–2.0 V vs. Li/Li^+ and are typically resilient enought so as to efficiently absorb the volume changes during charging/discharging process. Hence, an improved cycling and rate performance would be expected.

A Si/PEDOT: PSS composite prepared by *in-situ* polymerization of 3,4-ethylenedioxythiophene (EDOT) in the presence of nano-silicon dispersed in aqueous PSS [41] showed an initial discharge capacity of 1096 mAh/g first cycle coloumbic efficiency of 85%. The composite maintained a discharge capacity of 664 mAh/g after 20 cycles, but it decreased to 257 mAh/g after 50 cycles. Jie-Jian Cai *et al.* [24] reported on a nano-silicon/polyaniline composite by embedding silicon nanoparticles into the nest-like polyaniline matrix. The composite exhibited good cyclability and an improved capacity due to the better dispersion of silicon particles and increased conductivity of the composite.

S.Y. Chew and colleagues [55] demonstrated a novel nano-silicon/polypyrrole composite prepared by *in-situ* polymerization of pyrrole. The cycling stability of Si/PPy electrodes was greatly improved in comparison to that of the pure Si anodes. The PPy matrix provided a vast network forming a composite with increased electrical conductivity and good capacity for

buffering the large volume changes of silicon nanoparticles upon lithiation/de-lithiation, which prevented cracking and pulverization of the Si electrode.

The improved performance of the silicon-conductive polymer matrix composite anodes could be attributed to:

a) The conductive polymer matrix increases the conductivity of the Si electrodes;
b) The polymer matrix acts as "bridges" joining the silicon particles, which decreases the resistance between particles and reduces the irreversible reactions between particles and electrolyte;
c) The intrinsic resilient property of polymer matrix buffers the volume change during the lithiation/de-lithiation processes;
d) The conductive polymer matrix acts as an efficient host to prevent cracking and pulverization of the entire Si electrode, improving cyclability [55].

Hence, the use of conductive polymer matrices is an effective solution to overcome the drawbacks inherent to silicon anodes. Finding a suitable polymer matrix for the silicon composites is still a critical factor.

2.5.1.4 Other factors that influence the performance of silicon anodes

Beyond introducing different functional materials to the silicon anodes, several variables can be manipulated so as to improve its performance, including: type and amount of binders and conductive materials, current collectors and separators, particle size and micro/nanostructures of silicon composites and voltage control.

Applying various binders to the silicon anodes

By forming cross-links and providing adhesion between anodes and current collectors, binders provide an efficient pathway for electrons to pass through within the electrode. Besides PVdF that has been widely used as a binder material LIBs, some other binders have also been studied for silicon composite anodes, such as sodium carboxymethylcellulose (Na-CMC), rubber-like ethylene propylene diene monomer (EPDM), Oppanol B200 (BASF), polyethylene glycol with lithium perchlorate (PEG–$LiClO_4$), polyethylene oxide with lithium perchlorate (PEO–$LiClO_4$) and styrene butadiene rubber (SBR) [56-58].

Ning Ding and colleagues [59] compared the electrochemical performance of silicon anodes prepared with different binders (PVDF and Na-CMC) and concluded that Na-CMC afforded better performance than PVDF due to the esterification between hydroxyl on Si surface and carboxyl in Na-CMC.

With the aid of these binders (Na-CMC, SBR and etc.), the capacity retention of silicon composite anodes was greatly improved possibly because of better cross-linking and adhesion properties provided by these binders. The stability of these binders during charging/discharging process should also be taken into consideration.

Voltage control for the silicon anode materials during charge/discharge process

Michel Ulldemolins *et al.* [60] reported a "memory effect" for the silicon anodes if the discharge cut-off voltage for the involved anodes is lower than or equal to 50 mV versus Li^+/Li. The authors pointed out that after a certain amount of lithium was reacted, a progressive loss of capacity and reducing efficiency was observed upon cycling. This phenomenon was clearly observed when the crystallized phase $Li_{15}Si_4$ was formed. The researchers suggested that balancing capacities of negative and positive electrodes is crucial to avoid such "memory effect" in LIBs. They also inferred that the most efficient way to oversize the Si electrode capacity is maintaining the charge cut-off voltage above 100 mV during cycling of a full battery. It has also been suggested that lithiated amorphous Si will be suddenly converted to crystalline $Li_{15}Si_4$ when the cut-off voltage is lower than 50 mV. This results in high internal stress and capacity fading. The cyclablility and capacity retention can also be improved if the upper cut-off voltage of a nano-Si anode is reduced from 2V to 0.8V.

The disadvantage of voltage control in silicon anodes is that it reduces capacity. For example, increasing the lower cut-off voltage from 0V to 0.2V of an amorphous Si anode resulted in the specific capacity decreasing from over 3000 mAh/g to around 400 mAh/g [54].

Controlling the particle size of the silicon composites anodes

It has been confirmed in many studies that reducing the particle size of active material to nanometer scales (<100 nm) can significantly improve the cycling performance of silicon anodes, especially when a composite matrix is used to inhibit the agglomeration of silicon nanoparticles.

Ning Ding and co-workers [59] compared the electrochemical performance of silicon anodes with different particle sizes (74μm and 50nm) and concluded that nano-Si displayed a better electrochemical performance than that of microscopic silicon. The authors claimed that the nanosized particles allow more free space in the anode to accommodate the volume changes and have the ability to hold large stress and strain without cracking. In addition, the electronic and ionic transport length decreases as the particle size becomes smaller, reducing the strain induced by inhomogeneous Li diffusion [54]. Since nanocomposites have higher density of grain boundaries compared to bulk silicon, faster diffusion of Li ions is expected. However, nanosized particles have many disadvantages including large surface area, high manufacturing cost, and handling difficulties. Larger surface area results in more side-reactions and SEI formation, which may compromise cycling life. One possible way to overcome these problems is to prepare anode composites comprised of both large primary particles and nanosized secondary particles.

Applying advanced micro/nanostructures to silicon composite anodes

In recent years, researchers successfully developed advanced micro/nanostructures of silicon composite anodes with reduced capacity loss and improved performance. This can be approached in two ways:

a) Apply micro/nanostructure to silicon [37];
b) Introduce micro/nanostructured components to the silicon composites [61-63].

Cui *et al.* [61] created an amorphous silicon coated core-shell carbon nanotube composite anode, using the carbon nanotube as a backbone to support the high capacity silicon layer. The composite showed a good cyclability with capacity around 2000 mAh/g for over 50 cycles. A special 3D hierarchically structured silicon coated carbon nano-composite anode, with about 50 % silicon content, that exhibited an initial discharge capacity of 1950 mAh/g at C/20 rate was reported by Magasinski *et al.* [62].

Juchen Guo and colleagues [63] synthesized a silicon-porous carbon composite through a one-step carbonization of Si-poly (acrylonitrile-co-methyl acrylate) precursor. The composite was directly deposited on a carbon fiber mat current collector and the electrode demonstrated good overall capacity, cyclability, and rate performance. The discharge and charge capacities in the

first cycle were 728 mAh/g and 519 mAh/g, respectively, with irreversible capacity of 28.8%. The composite maintained an overall discharge capacity of 650 mAh/g after 100 cycles.

2.5.2 Silicon only anodes for Lithium-Ion Batteries

As discussed in earlier sections, the use of bulk silicon as anode for LIBs is impractical. Nonetheless, the use of recently developed advanced techniques of synthesis of nano-structured materials to prepare bulk silicon anodes (without binders, conductive material, or other additives) has brought a major breakthrough in the field, allowing the achievement of high capacity and good cycleability. Usually, the bulk silicon are prepared in structures that can be classified into three categories: 1-D structures, such as silicon nanowires; 2-D structures, such as silicon thin film; and 3-D structures, such as silicon nanotubes, porous silicon, silicon with hollow structure, silicon with yolk shell structure and other 3-D engineered structures.

◆1-D silicon structure

Silicon nanowires

Silicon nanowires (SiNWs) have attracted great deal of attention for applications in LIBs anodes due to their superiority over silicon powder [64]:

a) Facile strain relaxation allows silicon nanowires to accommodate massive volume change during repeated cycling without cracking [64];
b) 1-D structure of silicon nanowire provides an efficient pathway for electron transport;
c) Direct contact between nanowire and current collector improves the electrical conduction of the electrode;
d) Effective lithium insertion and extraction could be afforded due to the contact of lithium ions with large surface area.

Silicon nanowire anodes (Figure 2.5(b)) synthesized by Vapor-Liquid-Solid (VLS) technique exhibit capacities near the theoretical value for silicon (4200mAh/g). As shown in Figure 2.5 (a), Si nanowires synthesized by VLS technique did not experience significant pulverization or detachment from the current collector during repeated lithiation/de-lthiation, maintaining a reversible capacity of 2000 mAh/g for over 80 cycles. However, because of the expensive and

complicated preparation procedure, commercialization of this material is impractical [64]. Using an electroless-etching technique Helmut and co-workers [65] synthesized silicon nanowires, with a plated copper layer that behaved as mechanical support and current conductor. The anode showed good cycleability for over 10 cycles, however, the reversible capacity was not comparable to that of silicon nanowire synthesized by VLS technique.

Peng *et al.* [66] prepared self-aligned silicon nanowires by metal assisted etching. This method has several advantages over the VLS technique: low cost, large surface area, and facile procedure. The third cycle discharge capacity of the silicon nanowire anode was about 0.5 mAh/cm^2 and it maintained good cycling stability for up to 9 cycles. However, due to difficulties in estimating the weight of the silicon nanowires on the substrate, the reported capacity could not be compared with that obtained for silicon nanowires synthesized by VLS technique. In addition, because the nanowires are attached to the silicon substrate, lower electrical conductivity between anode and current collector is expected and the substrate may pulverize and crack after repeated cycling. These disadvantages limit the practical applications of the metal assisted method for preparation of LIB anodes.

Several surface modified silicon nanowires with improved cyclability have also been reported. The most common examples involve coat the silicon nanowires with conductive materials, such as carbon and copper, to increase conductivity. Huixin Chen *et al.* [67] synthesized copper coated silicon nanowires through vapor deposition and magnetron sputtering methods. The copper-coated SiNWs anode exhibited initial capacity of 2700mAh/g and coulombic efficiency of 90 %, at current density of 210mA/g. The improved performance was attributed to an indirect stabilization of the SEI, as a result of the suppression of deposition of the electrolyte decomposition products on the silicon surface, which in turns prevent pulverization of SiNWs. Additionally, the conductivity of copper and copper silicon alloy is higher than that of silicon, which is beneficial for a well distribution of the electric field so that polarization is alleviated.

A novel self-aligned Cu–Si core-shell nanowire array was fabricated by Qu and colleagues [68] *via* a low-temperature catalyst-free process. The copper core functioned as the backbone to impart mechanical strength and as an internal current collector to provide nanoscale electron transport

pathways. The material demonstrated good capacity retention with high coulombic efficiency. No wire fracture or core–shell separation was observed after cycling. However, the electrolyte decomposition products on the surface of the nanowires restricted electrolyte access, which resulted in capacity fading at higher rates.

However, the SINWs approaches described up to date are expensive and suffer from technical drawbacks like poor control of the pore volume, wire diameter, length, and uniformity and the weak adhesion to substrate. Hence, more work is still needed to solve these problems and drive the application of silicon nanowires into commercialization.

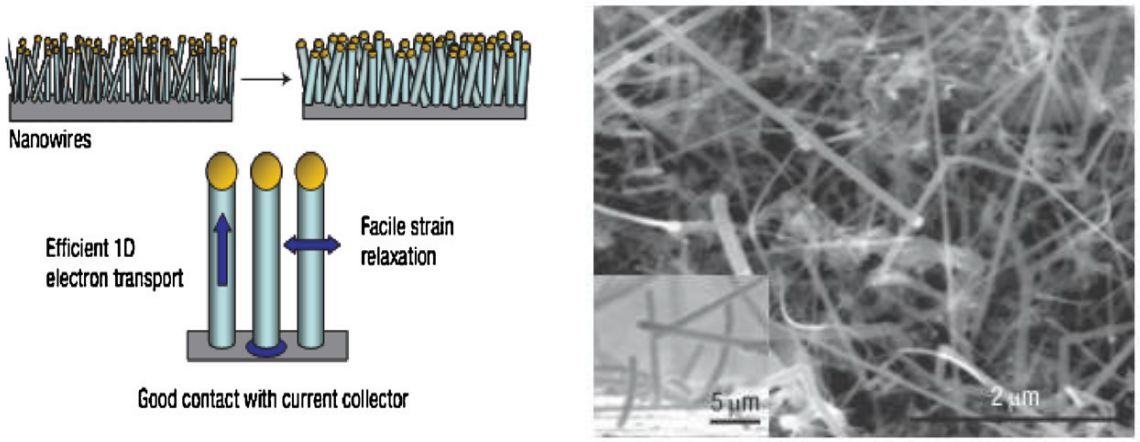

(a) **(b)**

Figure 2.5 (a) Concept schematic of Si nanowire electrode assembled on the current collector: (b) Scanning electron micrograph of Si nanowires (Reprinted by permission from Macmillan Publishers Ltd., High performance lithium battery anodes using silicon nanowires by Chan *et al.*, [Nature Nanotechnology], copyright 2008) [64].

◆2-D silicon structure

Silicon thin film

Methods such as chemical and physical vapor deposition, magnetron sputtering, pulsed laser deposition, and vacuum evaporation have been successfully employed to fabricate silicon thin film anodes for LIBs [69-78]. The assembly of ultrafine silicon materials into a continuous film constitutes an effective approach to overcome the volume change issue, enhance the contact area, and suppress the movement of free silicon particles.

Studies have been conducted on silicon thin film anodes in order to evaluate the lithium insertion mechanism [70], the stress evolution within the anode upon cycling [71-72], and surface film formation [73]. Even though cracking and pulverization were still observed on thin film silicon anodes after prolonged repeated lithiation/de-lithiation (Figure 2.6), the reversibility and capacity retention of the silicon thin film anodes are greatly enhanced. Recent studies showed that ultrathin silicon films (50nm thickness) delivered a reversible specific capacity of ~3500 mAh/g for over 200 cycles whereas films with 150 nm thickness could only provide 2200 mAh/g for 200 cycles [74]. Using radio frequency magnetron sputtering technique, Hong Guo and colleagues [33] fabricated 300nm thick silicon film anodes that exhibited reversible specific capacity of 3500 mAh/g and 90 % retention after 25 cycles. Wei Chen *et al.* [69] took advantage of photosintering process and successfully fabricated silicon films anodes for LIBs. The Ag modified thin Si films exhibited the remarkable initial specific capacity of 4301mAh/g with a good cyclability. The material maintained capacity at around 2090mAh/g after 30 cycles. The authors inferred that addition of silver nanoparticles improved the conductivity of silicon film and facilitated the formation of amorphous phase.

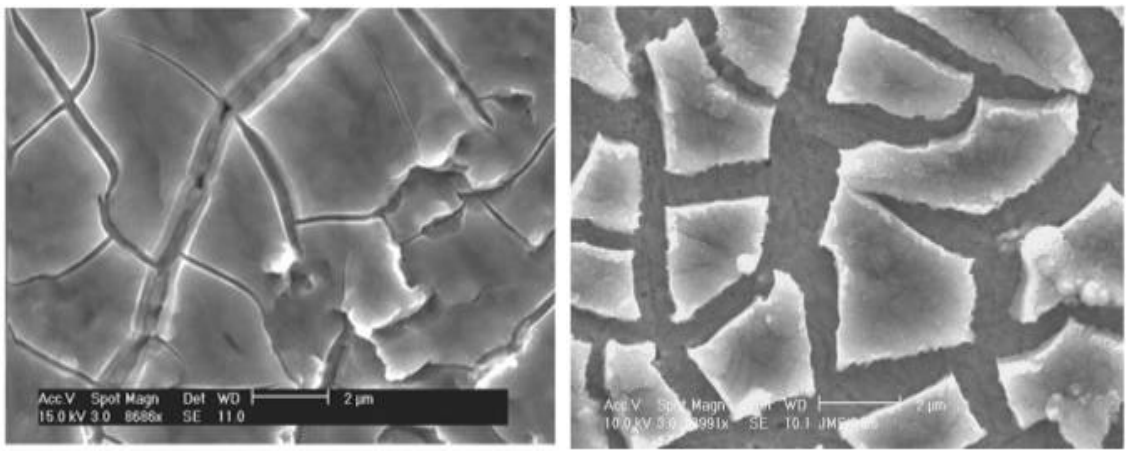

(a) **(b)**

Figure 2.6 (a) Stress-induced cracking of amorphous Si thin film after a few cycles; (b) Amorphous Si thin film-Delamination and peeling off from current collector after extended cycling (Reprint with permission from Electrochemical Society, Interfacial properties of the a-Si/Cu: active-inactive thin film anode system for lithium-ion batteries by J. P. Maranchi *et al.*, [J. Electrochem. Soc.], copyright 2006) [75]

Many attempts have been made to enhance the electrochemical performance of silicon film anodes [76-78]. Researchers introduced conductive elements such as silver, copper, and gold into silicon films to increase the conductivity [76]. Unique structures [77-78], such as nanomountain arrays and 3D porous film (Figure 2.7), have also been created within the silicon film to provide short electron pathways in order to enhance the rate performance of silicon thin film anodes. Most microscopic silicon film anodes display unstable capacity over prolonged cycling. As the film thickness increases, the stress-induced cracking and the high inherent resistance increases, resulting in poor cyclablility and rate performances. However, preparation of silicon thin films through expensive CVD or PVD techniques involves usage of toxic silanes as silicon source and strict operation conditions (high vacuum and high temperature), limiting the practical application of silicon thin film anodes.

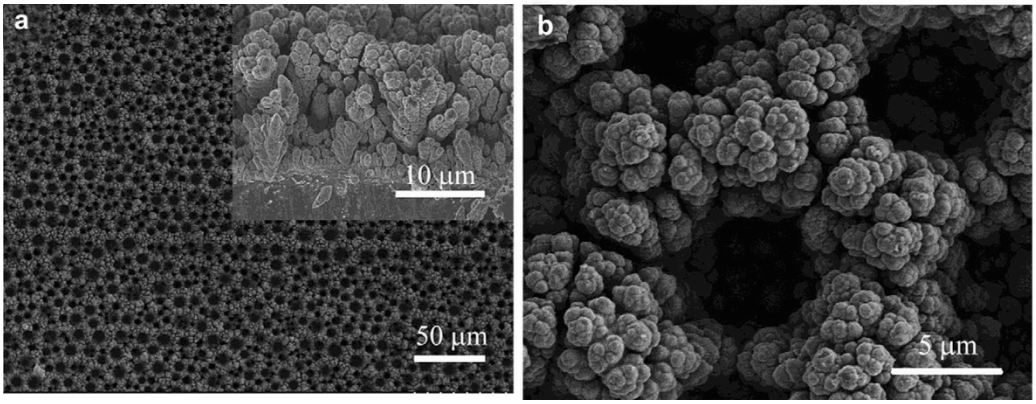

Figure 2.7 SEM images of 3D porous nano-Ni film (Reprint with permission from Elesvier, Three-dimensional porous nano-Ni supported silicon composite film for high-performance lithium-ion batteries by Y.Q. Zhang *et al.*, [Journal of Power Sources], copyright 2012) [78]

◆3-D silicon structure

Three dimensional structured electrode materials may provide significant improvement in both energy and power density of LIBs. Hence, much attention has been devoted in the development of electrodes with 3-D structures for the next generation LIBs [67-69]. Typically, electrodes with 3-D structure expose their active surfaces to the electrolyte in three dimensions, leading to a more effective utilization of the active materials. Furthermore, different 3-D structures could deliver different energy densities.

Porous silicon as anode material

Shin *et al.* [79] successfully prepared porous silicon anodes using an electrochemical etching process. The results showed that an increase in the channel depth of the porous silicon resulted in increased capacity. However, the specific capacity of the porous silicon anodes increased with the degree of pre-activation at the expense of cycling stability. A nano-porous Si/graphite/C composite was successfully synthesized by Zheng and colleagues [80] through a two-step ball milling and etching process. The nano-porous Si/graphite/C composite exhibited stable 700 mAh/g reversible capacity for up to 120 cycles at a constant current density of 0.2 mA/cm^2. The enhanced electrochemical performance of the nano-porous Si/graphite/C composite was attributed to the good electrical and ionic conductivity of the carbonaceous materials and to the nanosized pores within the Si particles, which buffer the severe volume change.

Wang *et al.* [81] prepared a series of porous Si/C composites employing diatomite as precursor, using low temperature magnesiothermic reduction and subsequent impregnation and carbonization of phenolic resin. Microscopy analysis revealed that the porous Si/C composites were coated with a 15 nm thick amorphous layer of carbon. The composite with 33% carbon content exhibited the highest initial specific capacity (~1628 mAh/g) and excellent capacity retention. The porous Si/C composite anodes also showed improved performance at high current densities (1A/g and 2 A/g).

Silicon nanotubes

An alternative silicon anode configuration with nanostructured geometry is silicon sealed nanotube (NT) layouts. Song *et al.* [82] developed arrays of sealed silicon nanotubes that exhibited high initial coulombic efficiency (> 85%) with stable capacity retention (> 80% after 50 cycles). The authors suggested that the system operates under unusual mechanics that is dominated by free surfaces, manifested by a strongly anisotropic expansion in which 400 % volumetric increases are accomplished with only relatively small (< 35%) changes in the axial dimension [82]. These experimental results demonstrated the advantage of bringing nanoscale engineering of electrode geometry into the Lithium-Ion Batteries design. Jaehwan Ha and colleagues [83] fabricated hydrogen treated cap-opened Si nanotubes arrays by first synthezing

sealed Si nanotubes *via* reactive ion etching (RIE) using chlorine plasma, followed by hydrogen treatment. The geometry of cap-opened Si nanotubes could provide the shorter lithium diffusion length and higher lithium ion flux compared with the sealed Si nanotubes [83]. The hydrogen treated cap-opened Si nanotubes electrode showed improved rate capability performance, delivering up to 61 % of the full capacity (obtained at low current density) at 1 C, which was 15 % higher than that of the sealed Si nanotube anodes.

A unique double walled silicon nanotube (DWSiNT) was designed by Wu *et al.* [84] to address the volume change and SEI stability issues of the silicon anode (Figure 2.8). The DWSiNT displayed good cycle life (6,000 cycles) with high capacity retention (88%), high specific capacity (2971mAh/g at C/5 and 940 mAh/g at 12C) and fast C rates for charge/discharge process (up to 20C).

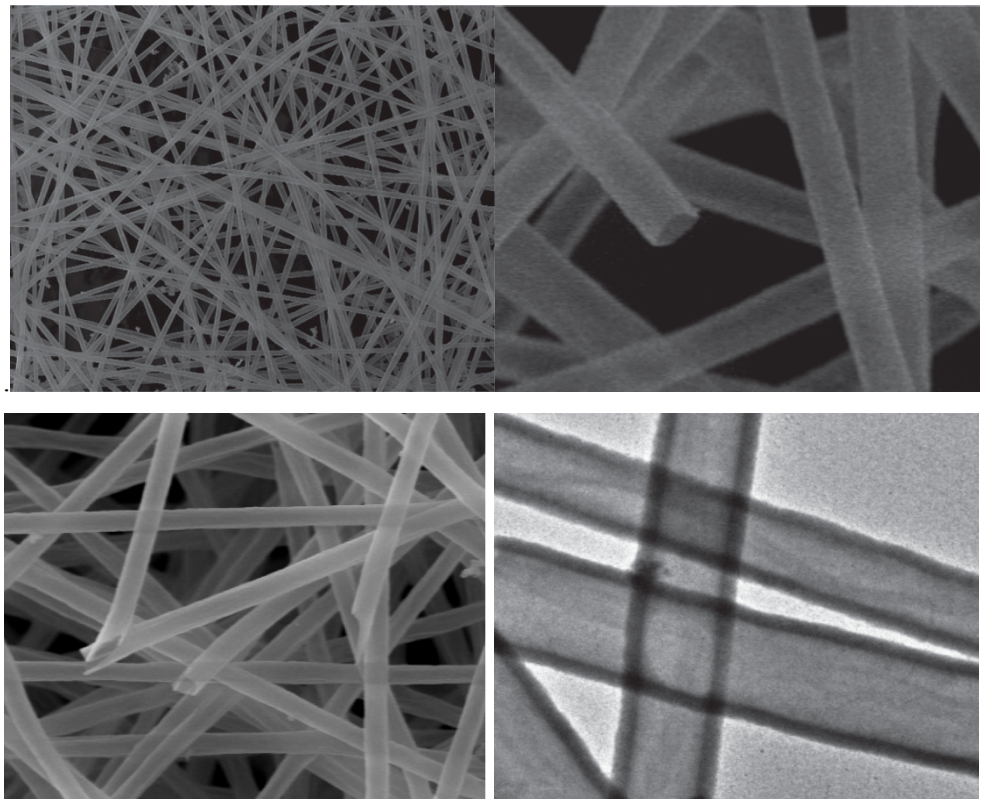

Figure 2.8 SEM and TEM images of synthesized DWSiNTs (Reprint with permission from Macmillan Publishers Ltd, Stable cycling of double-walled silicon nanotube battery anodes through solid–electrolyte interphase control by Hui Wu *et al.*, [Nature nanotechnology], copyright, 2012) [84]

Besides as-mentioned nanoscale architectures for applications in LIBs, the design and fabrication of such architectures provide the new approach for further improvement in electrode design and fabrication. It will be promising to apply such design to silicon alloy anode materials (SiGe, SiSn, SiAl, and SiSb alloys) or Silicon with other lithium inactive metals (Cu, Ni, and Co).

Silicon anodes with hollow structures

Hollow structures could provide more internal empty space allowing for the volume expansion. In addition, the hollow structures also relieves to stresses induced by low diffusion. Yao and colleagues [85] synthesized a Si hollow nanosphere electrode through a template method (Figure 2.9). The anode showed high initial discharge capacity of 2725 mAh/g with less than 8% capacity degradation every hundred cycles for 700 cycles and 99.5% coulombic efficiency. The improved electrochemical performance was attributed to fast lithium diffusion within the interconnected Si hollow structure. Alternatively, Si nanoparticles encapsulated in carbon shell showed superior electrochemical properties [86]. Because of its versatility, this structure could also be applied to the design of other high-capacity electrode materials that undergo large volume variations and poor cyclability. However, the synthesis procedure includes several relatively expensive steps and the usage of toxic hydrofluoric acid.

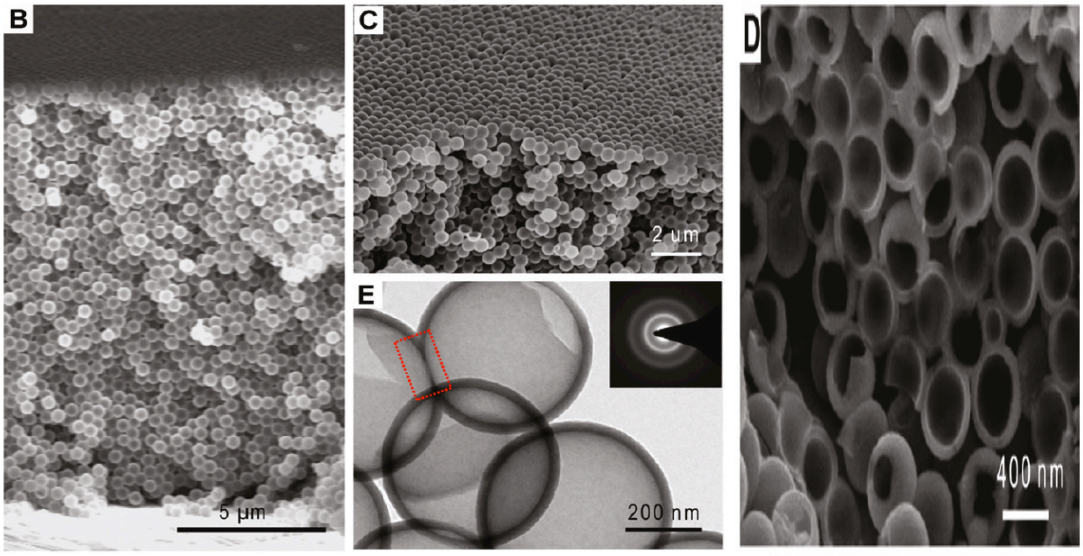

Figure 2.9 Typical cross-sectional SEM images and TEM images of hollow Si nanospheres (Reprint with permission from American Chemical Society, Interconnected Silicon Hollow Nanospheres for Lithium-Ion Batteries Anodes with Long Cycle Life by Yan Yao *et al.*, [Nanoletter], copyright 2011) [85]

Silicon with yolk shell structure

A yolk-shell structured silicon anode (Figure 2.10), consisting of Si nanoparticles sealed inside a thin and self-supporting carbon shell, was successfully prepared at room temperature without the use of any special equipment [87]. Because the Si particles could expand freely in the internal void space without breaking the outer carbon shell, the SEI on the shell surface was stabilized. The anode delivered high capacity (~ 2800 mAh/g at C/10) with a long cycle life (1000 cycles) and 74% capacity retention. High coulombic efficiency of 99.84% was also observed for this yolk-shell structured Si electrode.

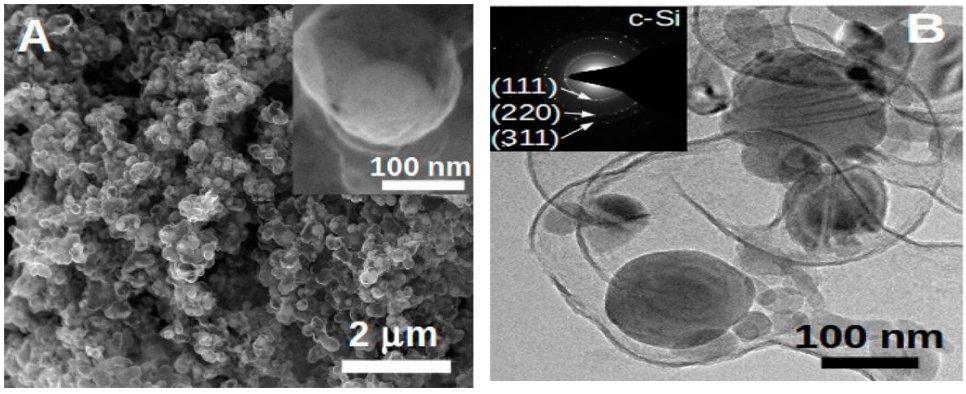

Figure 2.10 (A) SEM and (B) TEM images of synthesized yolk-shell structured silicon anode (Reprint with permission from American Chemical Society, A Yolk-Shell Design for Stabilized and Scalable Li-Ion Battery Alloy Anodes by Nian Liu et al, [Nanoletters], copyright 2012) [87]

Other silicon engineering structure

Hui Wu et al. [88] manufactured carbon nanotube encapsulated Si anodes using electrospinning methods. The space between the Si nanoparticles allowed for expansion and contraction without aggregation of the Si particles. The anode displayed high gravimetric capacity of about 1000 mAh/g (based on the total mass) with a long cycle life up 200 cycles and 90% capacity retention.

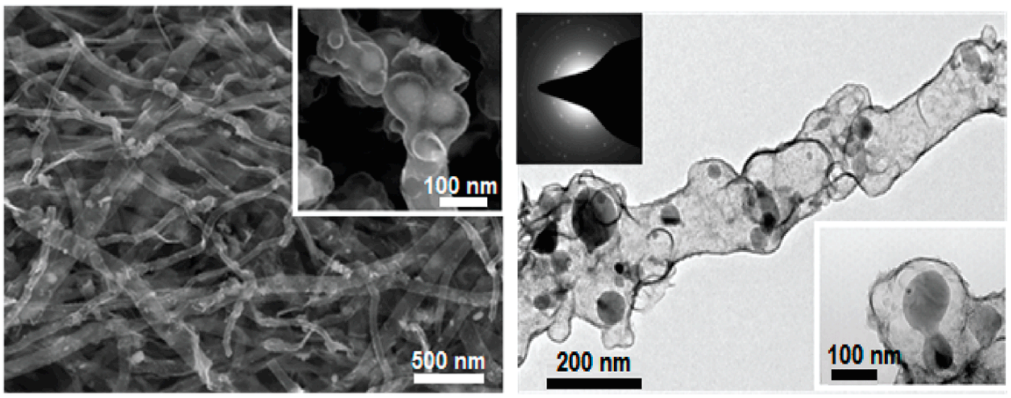

Figure 2.11 SEM and TEM images of a carbon nanotubes encapsulated Si anode (Reprint with permission from American Chemical Society, Engineering Empty Space between Si Nanoparticles for Lithium-Ion Batteries Anodes by Hui Wu et al, [Nanoletters], copyright 2012) [88]

The aforementioned architectures provide a new approach for further improvement in design and fabrication of electrode for LIBs, especially for silicon based anodes. For example, these approaches can be applied to design silicon alloy anode materials (SiGe, SiSn, SiAl, and SiSb alloys) or silicon within lithium inactive metals (Cu, Ni, and Co). As discussed above, nanostructured composite and bulk silicon anodes achieved commendable electrochemical performance. Nevertheless, the study and design of silicon anodes is still an area demanding intense work, especially regarding the following aspects:

a) The quantitative understanding of nanoscale design.
b) The nature of the solid electrolyte interphase on Si surface. The SEI influences the coulombic efficiency and the first cycle irreversible capacity of the silicon material. Nanoscale coating of Si maybe an efficient strategy to improve the stability of solid electrolyte interphase on Si surface.
c) The mechanism for lithium insertion and extraction to/from Si in atomic scale. The use of advanced *ex-situ* or *in-situ* characterization techniques associated with multi-scale modeling and simulation may prove helpful to unveil such processes.
d) Methods of packing nanostructured Si into the electrode structure.
e) Deformation mechanisms at the electrode level [25].

2.6 Solid Electrolyte Interphase

◆Electrolyte

The electrochemical performance for the LIBs depends strongly on the selection of the electrolyte for the battery system. The electrolyte acts as an ionic medium for lithium transport between the anode and cathode during charge/discharge process. In general, the electrolytes for the LIBs comprise of lithium salts dissolved in organic solvents. Lithium aprotic compounds, such as lithium hexafluorophosphate ($LiPF_6$), lithium hexafluoroarsenate ($LiAsF_6$), lithium Bis(Oxalato)Borate (LiBOB), lithium tetrafluoroborate ($LiBF_4$) etc, are usually used as lithium ion source. The lithium salt is dissolved in an alkyl carbonate solvent or mixture (e.g. ethylene carbonate (EC), dimethyl carbonate (DMC), diethyl carbonate (DEC), ethyl methyl carbonate (EMC), etc) to form a lithium salt organic solution [89]. These electrolytes are highly moisture sensitive so they must be produced under rigorous conditions to prevent side reactions upon battery operation. Some common carbonate solvent structures are showed in Figure 2.12.

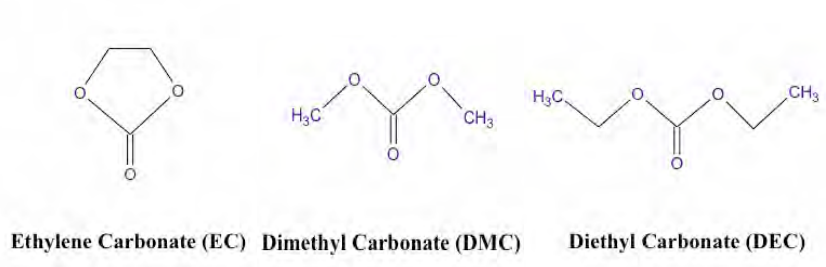

Figure 2.12 Alkyl carbonate solvent structures [3]

The reactions on the anode surface usually involve carbonate solvent, lithium salt, and contaminants such as dissolved oxygen, water, and carbon dioxide under anodic polarization [3]. The products from the surface reactions on graphite anodes have been identified, and the mechanisms of the surface reactions have also been extensively studied [90]. Aurbach *et al.* [91] proposed a possible mechanism for EC reduction on graphite anodes. A continuous passivating organic film is generated by the products of EC and other organic solvents reacting with lithium ion under cathodic bias through several steps (Figure 2.13).

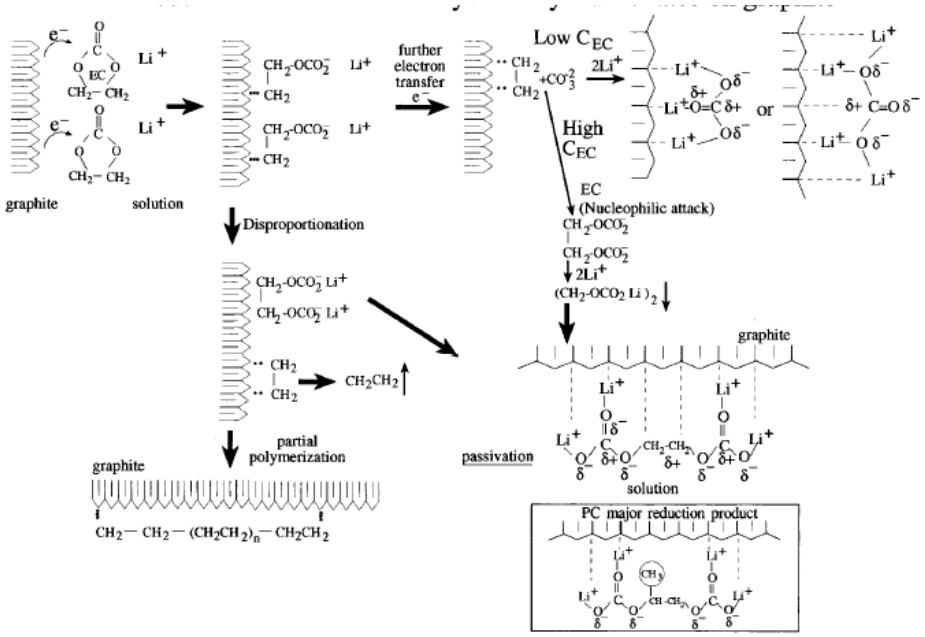

Figure 2.13 Various EC reduction patterns on graphite anode surface and relevant products (Reprinted with permission from Elsevier, On the correlation between surface chemistry and performance of graphite negative electrodes for Li ion batteries by Aurbach *et al.*, [Electrochimica Acta], copyright 1999) [91]

The reactions of lithium hexafluorophosphate, organic solvents and their derivatives on carbon anodes could be summarized by the following chemical equations [90]

$2EC + 2e^- + 2Li_+ \rightarrow CH_2{=}CH_2 + (CH_2OCO_2Li)_2$

$DMC + e^- + Li^+ \rightarrow CH_3OCO_2Li + CH_3\bullet$ or $CH_3OLi + CH_3OCO\bullet$

$DEC + e^- + Li^+ \rightarrow CH_3CH_2OCO_2Li + CH_3CH_2OLi$

The reduction products may react with traces of water in the electrolyte according to the following [3]:

$2ROCO_2Li + H_2O \rightarrow Li_2CO_3 + 2ROH + CO_2$

Lithium salts (e.g. $LiPF_6$) may also undergo surface reactions with very small amount of contaminant water in the electrolyte [3]:

$LiPF_6 \leftrightarrow LiF + PF_5$

$PF_5 + H_2O \rightarrow POF_3 + 2HF$

$POF_3 + 2xLi^+ + 2xe^- \rightarrow xLiF(s) + LixPOF3\text{-}x$

$PF_5 + 2xLi^+ + 2xe^- \rightarrow xLiF(s) + LixPF5\text{-}x$

$(CH_2OCO_2Li)_2 + H_2O \rightarrow Li_2CO_3 + CO_2 + (CH_2OH)_2$

$ROCO_2Li(s) + HF \rightarrow LiF(s) + ROCO_2H$

The carbon dioxide under anodic polarization may involve the following reducing reactions:

$CO_2 + e^- + Li^+ \rightarrow \bullet CO_2Li$

$\bullet CO_2Li + CO_2 \rightarrow O{=}\bullet CO\text{-}CO_2Li$

$O{=}\bullet CO\text{-}CO_2Li + e^- + Li^+ \rightarrow CO + Li_2CO_3$

$2LiOH + CO_2 \rightarrow Li_2CO_3 + H_2O$

$Li_2O + CO_2 \rightarrow Li_2CO_3$

$ROLi + CO_2 \rightarrow ROCO_2Li$

Note that R stands for alkyl functional groups such as $-CH_3$, $-CH_3CH_2$, etc.

◆SEI on Silicon Anodes

The SEI layer formed on silicon anodes greatly differs to that formed on the surface of graphite anodes mainly because:

a) The higher reactivity of the silicon surface in comparison with graphite: this leads to the formation of complex SEI composition including hydrocarbons, various lithium alkylcarbonates ($ROCO_2Li$), Li_2CO_3, Li_2O, LiF, some silicon containing products (such as lithium silicates, SiF_6^{2-}, etc.) and some nonconductive polymers [92-95].
b) The large volume change for silicon material upon cycling: this inhibits the formation of a dense and stable SEI layer on the surface of silicon anodes [25].

In addition to the surface reactions previously summarized for graphite anodes, some specific surface reactions were proposed to explain the SEI composition for silicon anodes: [25].

$SiO_x + 4HF + 2F^- + 2h^+ \rightarrow SiF_6^{2-} + 2H^+ + H_2O$

$SiO_x + 2xLi^+ + 2xe^- \rightarrow xLi_2O + Si$

$SiO^- + 2Li \rightarrow Li_2O + Si$

$SiO_x + Li^+ \rightarrow LiSO_x$

$EC + Li^+ + Si + e_- \rightarrow ROCO_2Li/Si$ + other carbonates

These specific irreversible reactions occurring on the surface of silicon anodes result in the consumption of lithium and silicon content and form some by-products that may block lithium transport, leading to capacity fading and poor rate performance [3, 57, 96-99]. An *in situ* analysis carried out by Flake *et al.* [100] showed that silicon oxidation products might strip fluoride from complexes, which cause the localized silicon etching process and increased production of LiF or other types of fluorinated by-products. Besides that, Song and co-workers [98] showed that irreversible oxidation reactions with fluorine on the silicon-SEI interface also influence the capacity fade of silicon thin film anodes.

Many approaches have been applied to alleviate the surface reactions on the silicon anodes. Among these, coating silicon with conductive carbons or other active/inactive materials were shown effective since the coatings work as both protection layers and conductive sources [31, 101-104]. The electrolyte can also be modified by the addition of additives to stabilize the SEI on silicon anodes. Choi et al. [105] improved the reversible discharge capacity of silicon anodes by 88.5% through the addition of 3 % fluoroethylene carbonate (FEC) in the electrolyte. Chen [106] found that the SEI layer formed on silicon anodes cycled in 1M lithium bexafluorophosphate (LiPF6) in a 1:1 (v/v) mixture solvent of ethylene carbonate (EC) and dimethyl carbonate (DMC) with 1 wt.% VC additive electrolyte possessed better properties than in VC-free electrolyte, namely, reduced amount of by-products on the silicon surface and decreased LiF content in SEI layer. Chen also discovered that, in both VC-free and VC-containing electrolytes, silicon oxide could be formed in SEI layer of Si film anodes due to the reaction between Li-Si alloys and permeated electrolyte.

The surface chemistry of the SEI greatly affects the electrochemical performance of anode materials. Although silicon surfaces are considered more reactive than that of graphite, the relationship between surface chemistry and anode performance is still not clearly established. Chan et al [92] compared the SEI formed on hydride-terminated silicon surfaces and nanowires with native oxides surfaces and established that nanowires with native oxides surfaces display 50 % more capacity retention than hydride-terminated anodes. The SEI compositions of the two silicon anodes were also significantly different. Peng *et al.* [70] discovered in their study that the surface chemistry affects the transport and adsorption of lithium while influencing the anode stability. Theoretical calculations in Peng's work predicted that the lithium transport rate was limited by a high energy barrier for lithium surface intercalation in the silicon thin film anodes. Surface modification by aluminum doping could reduce the barrier for silicon thin film anode.

As previously stated, the SEI is of great importance for silicon anode in terms of capacity retention and cycling stability. Since the surface science of SEI formed on silicon surface is still not clearly understood, more efforts are required to provide insight on the SEI formation mechanisms and product composition.

Chapter 3 Materials and Methods

3.1 Chemicals

The chemicals used in this work are showed in Table 3.1.

Table 3.1 Chemicals list

Name	Company	Grade	Concentration or assay
200 mesh Natural Graphite powder	Alfa Aesar	High purity	99.9999%
Sodium chloride	EMD	Analysis	99.0% min
Sulfuric Acid	EM Science	Analysis	95-98%
Potassiun Permanganate	EMD	ACS	99%
Sodium Nitrate	Sigma-Aldrich	Reagent Plus	≥99.0%
Hydrazine solution	Aldrich	Not provided	35w% in water
Ammonium Hydroxide solution	Sigma-Aldrich	ACS	28-30.0%
Hydrogen Peroxide solution	Sigma-Aldrich	ACS	30wt% in water
Cellu.Sep H1 cellulose membrane tube	Membrane Filtration Products, Inc.	High grade	None
Dodecyltrimethyl ammonium bromide	Sigma	Not provided	≥98%
Ammonium Persulfate	Sigma-Aldrich	ACS	≥98%

Aniline	Sigma-Aldrich	ACS	≥99.5%
1-Butanol	Sigma-Aldrich	HPLC	99.8%
Potassium Bromide	Fisher Scientific	IR grade	Not provided
Hydrogen Chloride Solution	Fisher Scientific	ACS plus	36.5-38.0%
(Selectilyte) Battery electrolyte LP40	EMD	Not provided	Not provided
Vinylene Carbonate	Aldrich	Not provided	97%
Lithium foil	Aldrich	Not provided	99.9%
Carboxymethyl cellulose sodium salt	Sigma	Not provided	Not provided

3.2 Composite preparation

The n-Si/PANi/RGO composite was synthesized *via* a two-step process: *in-situ* polymerization of polyaniline (PANi) in the presence of nano-silicon followed by combination of the prepared n-Si/PANi binary composite with reduced graphene oxide (RGO) to form a n-Si/PANi/RGO composite.

3.2.1 Preparation of nano-Si/polyaniline composite

In-situ polymerization of polyaniline (PANi) in the presence of nano-silicon was carried out in a DTAB/1-butanol aqueous solution. After sonication for 30 min of 0.3 g nano-silicon particles (US Research Nanomaterials, Inc.) in a solution of 0.5 g dodecyltrimethylammonium bromide (DTAB) surfactant and 0.375 ml 1-butanol co-surfactant in 100ml of deionized (DI) water a homogeneous brown suspension was obtained. A solution of 3.3 mmol of aniline monomer in 30 ml HCl (pH=1) was added drop wise to this suspension under vigorous stirring. Still under stirring, the mixture was immersed in an ice bath and a solution of 0.19 g ammonium persulfate (APS, 0.825 mmol) in 10 ml deionized water was slowly dropped into the mixture to initiate the *in-situ* polymerization of aniline. The system was kept under this condition for 24 hours after which the color of the mixture changed to greenish-brown. The precipitate was vacuum filtrated then thoroughly washed with ethanol, deionized water, and 0.15 mol/L HCl solution. The final powder was dried in a vacuum oven at 60 ^{o}C for 12 hours. This sample was labeled as n-Si/PANi.

3.2.2 Preparation of Reduced Graphene Oxide (RGO)

Graphite oxide was prepared through a modified Hummers method [110]. 0.8 g natural graphite was reacted with 23 ml concentrated sulfuric acid for 24 hr. Subsequently, 100 mg $NaNO_3$ was added to the mixture and, after stirring for 5 mins, 3 g $KMnO_4$ was slowly added to the mixture while the temperature of the system was kept below 20 ^{o}C in an ice bath. The suspension was diluted by the addition 200 ml DI water and heated up to 100 ^{o}C for 15 minutes, after which the reaction was terminated by the addition of 10 ml hydrogen peroxide. The resulting suspension was repeatedly centrifuged and washed with 5% HCl and DI water before a homogeneous brown graphite oxide solution was obtained. This solution was dialyzed against DI water to remove the

remaining metal ions. After dialysis, the graphite oxide aqueous suspension was sonicated for 30 minutes to obtain graphene oxide suspension which was diluted to 0.05 wt.% afterwards.

Reduced graphene oxide (RGO) sheets were obtained by the reduction of graphene oxide with hydrazine solution in the presence of ammonia solution. Typically, 100 ml of homogeneous 0.05 wt.% graphene oxide suspension were mixed with 100 ml DI water, 100 μL hydrazine solution, and 0.7 ml ammonia solution. The weight ratio of hydrazine to graphene oxide was about 7:10. While under vigorous stirring, the suspension was immersed in oil bath at 95 ^{o}C for 1 hour. The excess hydrazine was thoroughly removed by subsequent dialysis against 0.5% ammonia solution.

3.2.3 Preparation of nano-Si/polyaniline/ Reduced Graphene Oxide composite

The procedure for making nano-silicon/polyaniline/reduced graphene oxide composite was similar to that of n-Si/PANi, except that before the final wash and filtration steps, 200 ml 0.025 wt% RGO suspension was slowly dropped into the mixture in the presence of DTAB. The color of the suspension changed to black after this addition. After vigorous stirring for 12 hours, the suspension was subjected to the filtration and washing processes. The collected particles were dried at 60^{o}C in a vacuum oven for 12 hours to yield dark green particles. This sample was labeled n-Si/PANi/RGO. The schematic diagrams of the two procedures are shown in Figure 3.1.

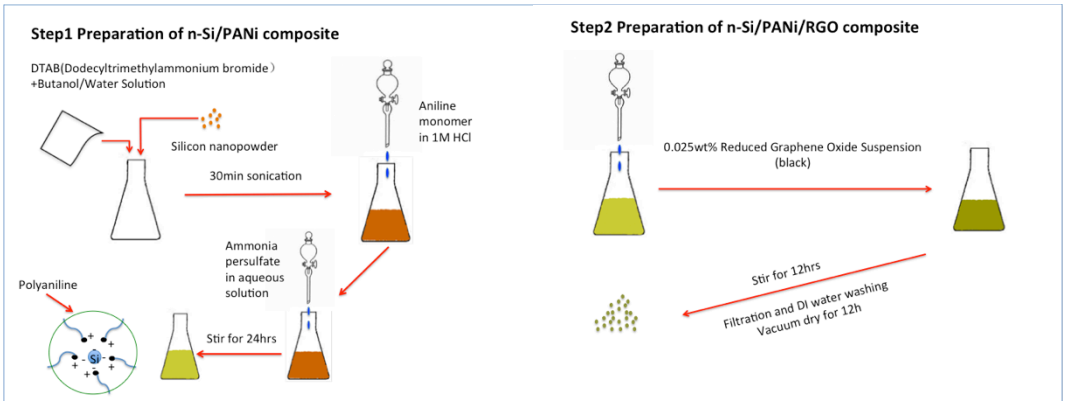

Figure 3.1: Schematic representation of (a) preparation of the n-Si/PANi composite and (b) combination of the as-prepared n-Si/PANi with RGO to form n-Si/PANi/RGO composite.

3.3 Material Characterization

3.3.1 Scanning Electron Microscopy (SEM)

Scanning Electron Microscope (SEM) analysis was carried out to study the morphology and structures of n-Si/PANi, n-Si/PANi /RGO composites and nano-Si. The scanning electron microscope (SEM) images the surface of the sample by scanning it with a high-energy beam of electrons. The electrons interact with the sample which produces signals containing information about the topography of a sample surface. SEM can produce images of a sample surface at very high-resolution (nm scale), however, it depends on specification of individual SEM system [107].

Nano-Si, n-Si/PANi and n-Si/PANi /RGO composites were applied to conductive tape respectively with very small amount which were attached to SEM sample holders and loaded into SEM chamber to conduct material characterization study. In this work, the Scanning Electron Microscopy analysis was carried out on a Leo FESEM scanning electron microscopy SEM/EDS system (Figure 3.2). All the images were obtained under 15 kV at various amplifications for later comparisons.

3.3.2 Transmission Electron Microscopy (TEM)

TEM emits a beam of high-energy electrons that transmit through a sample and interact with sample atoms to form images on a florescence screen. TEM could provide high-resolution images in nanometer scale and is useful for study crystal lattices and atomic layer structure. In this work, Transmission Electron Microscope (TEM) was applied to nano-Si, n-Si/PANi and n-Si/PANi /RGO composites to characterize and make comparisons of these three different materials. Small amount of nano-Si, n-Si/PANi and n-Si/PANi /RGO composites samples were dispersed in DI water respectively, which were followed by a 30 min ultrasonication. Then a small drop (10 μL) of each sample was deposited onto Formvar Coated 300 meshes Copper TEM grids (Canemco & Marivac). The grids were subjected to the tests after the grids were dried in atmosphere.

A Philips CM10 transmission electron microscope (Figure 3.3) was used for the material characterization.

Figure 3.2 Leo FESEM SEM/EDS system

Figure 3.3 Philips CM10 TEM system

3.3.3 Fourier Transform Infrared Spectroscopy (FT-IR)

Fourier Transform Infrared Spectroscopy (FT-IR) is a well-established technique to obtain specimen chemical composition by identifying specific bond structures of certain organic species [108].

Fourier transformed infrared spectroscopy analysis was conducted in transmission mode with KBr pellets at the resolution of 2 cm^{-1} for 16 scans on Bruker Vertex 70 FT-IR equipment (Figure 3.4) in this work. The recorded spectroscopic data was analyzed in OMNI software installed with the Bruker Vertex 70 FT-IR system.

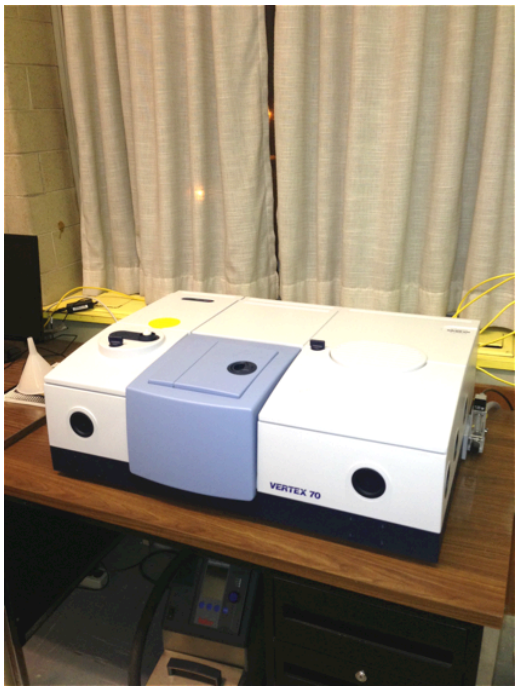

Figure 3.4 Bruker Vertex 70 FT-IR system

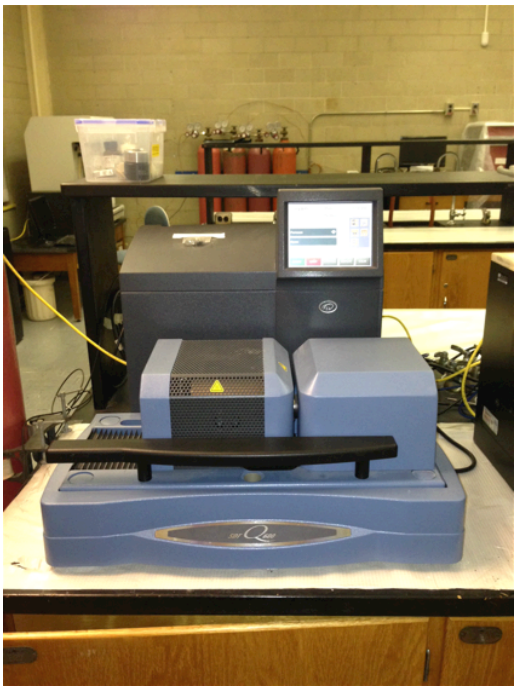

Figure 3.5 TA Instruments SDT Q600 TGA

3.3.4 Thermogravimetric analysis (TGA)

Thermogravimetric analysis is a thermal analysis method in which changes in physical and chemical properties of materials are measured and recorded as a function of increasing temperature, or as a function of time. TGA can provide information about chemical phenomena including chemisorption, desolvation (especially dehydration), decomposition and solid-gas reactions (e.g., oxidation or reduction) [109]. In this thesis, TGA was carried out on a TA Instruments SDT Q600 (Figure 3.5) in air atmosphere which was heated to 800°C at a rate of 3 °C/min to study the oxidation reaction on the silicon surface and decomposition of polyaniline and reduced graphene oxide, which was used for the calculation of the silicon contents in nano-Si, n-Si/PANi and n-Si/PANi /RGO composites.

3.4 Coin cell making

3.4.1 Preparation of slurry

The n-Si/PANi and n-Si/PANi/RGO composites and nano-silicon were mixed with acetylene black (AB) and carboxymethyl cellulose sodium salt (Na-CMC) respectively in a 75:10:15 weight ratio, which were grounded in agate mortars for 40mins in Deionized water at room temperature to form homogeneous slurries.

3.4.2 Electrode making

The as-prepared slurries were transferred to pre-sized (thickness) copper foils (repeated cleaned with ethanol) to form even thin films with 150μm thickness. Then the slurry-attached copper foils were dried in the atmosphere at room temperature before cutting into electrode (Ø= 11.70mm) with a precision disc cutter (Figure 3.6, MTI). The electrodes were dried in a vacuum oven together with CR2025 coin cell cases (Figure 3.7) at 100°C for 12 hrs under vacuum to remove the residual water.

3.4.3 Mass calculation for the active materials

The mass of the n-Si/PANi and n-Si/PANi/RGO composites and nano-Si were obtained by using a 6-digit microbalance (Figure 3.8 Mettler ToleDo XS105 microbalance, 0.01mg resolution). The weight of each electrode was measured by the microbalance respectively. Then the total weight of 5 void copper foil (as the same size as the electrodes) was measured by the same microbalance, which was divided by 5 to get the average weight value of each void copper foil. The mass of the material deposited on each electrode was obtained by minus the weight of void copper foil off the weight of electrodes. The mass of the active material in each electrode was achieved by multiplied 0.75 of as-calculated mass of the material deposited on each electrode.

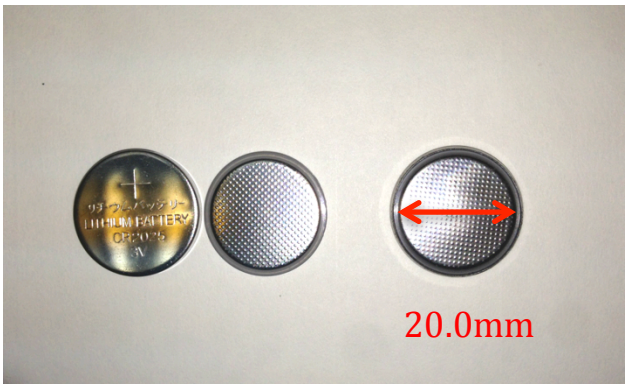

Figure 3.6 MTI Precision disc cutter

Figure 3.7 CR2025 coin cell sets

3.4.4 CR2025 coin cell assembly

Once the anode materials were dried, they were transferred to an Ar-filled glove box to be assembled against Li metal foils into CR 2025 coin cell sets (Figure 3.7). Since Li metal is extremely reactive with air and moisture, it was kept in the inert atmosphere to prevent the further reaction. The atmosphere in the glovebox (MBraun, Figure 3.9) consisted of argon, H_2O (<0.1ppm) and O_2 (<0.1ppm). A Microporous plastic film (Celgard 2250) was used as a separator to separate the Li metal foil and as-prepare electrodes. The electrolyte was a solution of 1 M $LiPF_6$ in ethylene carbonate (EC)/diethyl carbonate (DEC) (1:1 by weight, (Selectilyte) Battery electrolyte LP40, EMD) and 2wt% vinylene carbonate (VC, Sigma-Aldrich) as electrolyte additive. After assembly, the coin cell was tested for the open circuit voltage (around 2.5 V). It should be noted that when Li metal was used as counter electrode for these half-cells, the as-prepared electrodes actually behaved as a cathode at this point since Li has the lowest electrochemical potential. However the principle of insertion and de-insertion of Li for the active materials still remained the same.

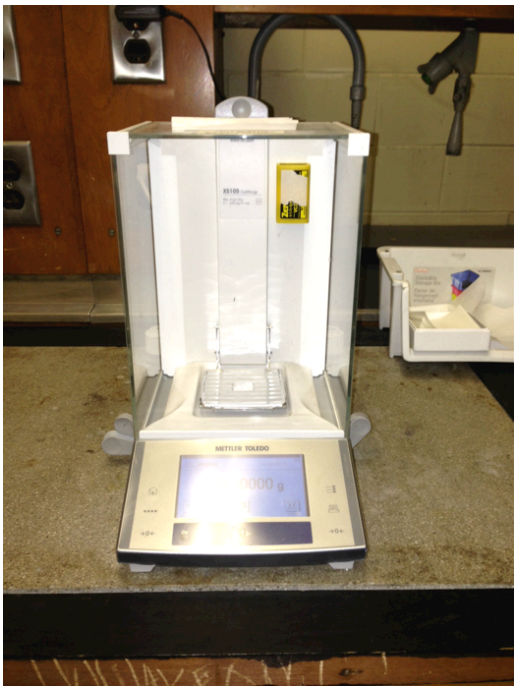

Figure 3.8 Mettler ToleDo XS105 microbalance

Figure 3.9 MBraun Labmaster SP Glovebox

3.5 Electrochemical characterization

The following techniques were conducted to evaluate the electrochemical performance of the three different anode materials, namely n-Si/PANi and n-Si/PANi/RGO composites and nano-Si.

3.5.1 Charge/Discharge cycling test

As-assembled cells were cycled with a constant current density (200mA/g) within fixed voltage limits between 0.01 V to 2 V. The magnitude of the constant current was calculated based on the Si content in each electrode. A multi-channel battery tester (Figure 3.10 Neware multi-channel battery tester, China) was used for this test.

3.5.2 Rate capability test

As-assembled cells were cycled with various current densities (200mA/g, 500mAh/g, 1000mA/g and then back to 200mAh/g) within fixed voltage limits between 0.01 V to 2 V. The magnitude of the constant current was calculated based on the Si content in each electrode. The same multi-

channel battery tester (Figure 3.10 Neware multi-channel battery tester, China) was used for this test.

3.5.3 Cyclic Voltammetry (CV) test

CV could give important information about the nature of the electrochemical alloying reactions that occur in the electrode. Cyclic voltammetry measurements were carried out on a Biologic VMP3 electrochemistry workstation in the range of 0.01V to 2V at a rate of 0.1mV/s. At certain voltages, one would observe peaks in the current response which could be attributed to specific electrochemical reactions that generate this current response. Therefore, by studying the CV plot, it is possible to identify which material alloys with lithium since different materials alloy with lithium at different electrochemical potentials. The Biologic VMP3 electrochemistry workstation (Figure 3.11) was used to conduct the CV test for this work.

3.5.4 AC impedance test

AC impedance measurements were carried out on a Bio-Logic VMP3 electrochemistry workstation (Figure 3.11) in the range of 0.1kHz to 100kHz for to study the internal resistance of nano-Si, n-Si/PANi and n-Si/PANi/RGO composites.

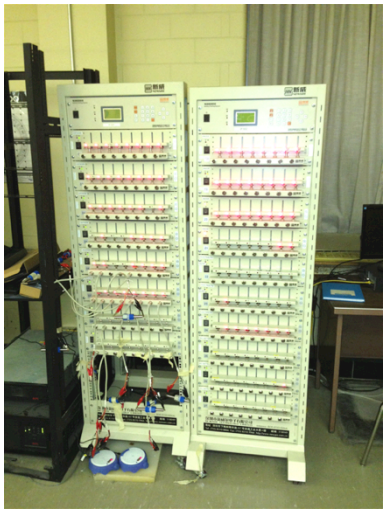

Figure 3.10 Neware multi-channel battery tester

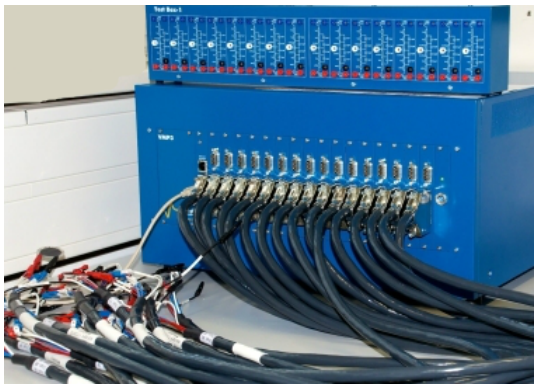

Figure 3.11 Biologic VMP3 electrochemistry workstation

Chapter 4 Results and Discussions

4.1 FTIR analysis

FTIR analysis was conducted to identify the functional groups and characterize the covalent bonding in polyaniline and reduced graphene oxide (Figure 4.1). Several characteristic peaks were observed in the n-Si/PANi/RGO spectrum, namely: the C=C stretching vibration of the quinoid rings at 1586 cm^{-1}; the band at 1499 cm^{-1}, attributed to the C=C stretch of benzenoid rings [111]; the C–N stretching of the secondary aromatic amine at 1300 cm^{-1} [24]; the absorption band at 1189 cm^{-1} is related to C-C stretching vibrations [112]. These results demonstrate the in-situ polymerization of aniline in the n-Si/PANi/RGO composite [113,114]. In addition to the characteristics bands of polyaniline, a peak emerged in FTIR spectrum of n-Si/PANi/RGO composite at 1575 cm^{-1}. It can be attributed to the aromatic C=C groups from RGO, suggesting that the RGO structure is still well preserved in n-Si/PANi/RGO composite. The lower wavenumber absorption band at around 620 cm^{-1} is assigned to Si-Si vibrations derived from the silicon particles, suggesting that silicon nanoparticles are preserved in the composite.

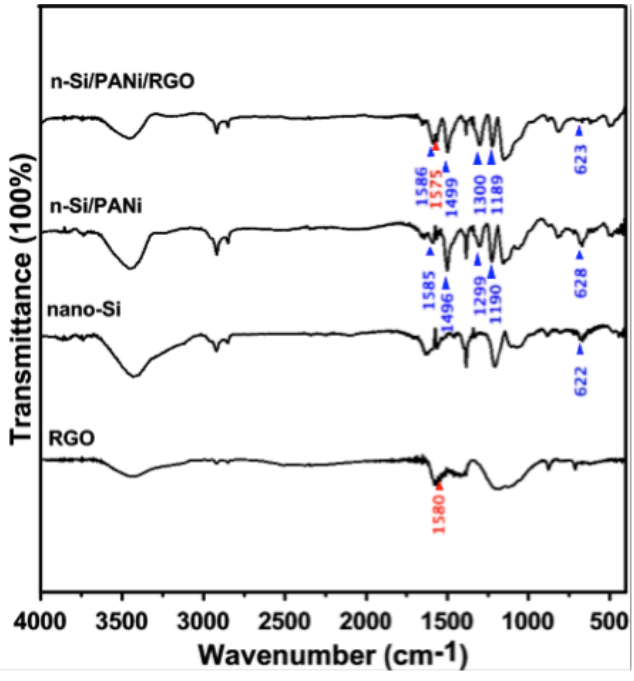

Figure 4.2: FT-IR spectrum of nano-Si, n-Si/PANi and n-Si/PANi/RGO composites

4.2 SEM images

Electron microscopy and x-ray energy dispersive analysis were conducted to investigate the morphology, structure, and composition of the phases. The SEM images at different magnifications are presented in Figure 4.2. Both nano-Si and n-Si/PANi show interconnected spherical particles. However, the average particle size of n-Si/PANi (80-120nm) is larger than that of nano-Si particles (40-80nm), indicating that the polymerization process occurred on the surface of the nano-Si particles. The characteristic wrinkled structure of reduced graphene oxide sheets is clearly observed in the SEM images of n-Si/PANi/RGO composite. Moreover, it seems that the nanoscopic Si particles are homogeneously deposited on the RGO sheets, since no empty sheets were found in the images. The nano-Si particles, reduced graphene oxide sheets and polyaniline conductive matrix form a homogeneous nano-architectured composite in which nano-Si is well dispersed. This morphology should hinder agglomeration of the nanoparticles, thus preventing pulverization upon cycling [43].

The EDX analysis（Figure 4.3 (a)(b)) shows that the nano-Si/PANi/RGO composite consist of C, N, O and Si with contents of 24.2%, 3.6%, 8.0% and 64.2% respectively (Table 4.1), which is close to the 68% Si content in nano-Si/PANi/RGO composite from TGA result (Figure 4.5). It should also be noted that polyaniline is the only N source for nano-Si/PANi/RGO composite, which implies that the in-situ polymerization has been successfully processed for nano-Si/PANi/RGO composite.

Table 4.2: Summary of EDX analysis result of n-Si/PANi/RGO composite

Element	Weight %	Atomic %	Net Int.	Net Int. Error
C K	24.24	39.9	91.55	0.03
N K	3.55	5.01	13.82	0.16
O K	8.01	9.9	107.8	0.03
SiK	64.2	45.19	2194.83	0

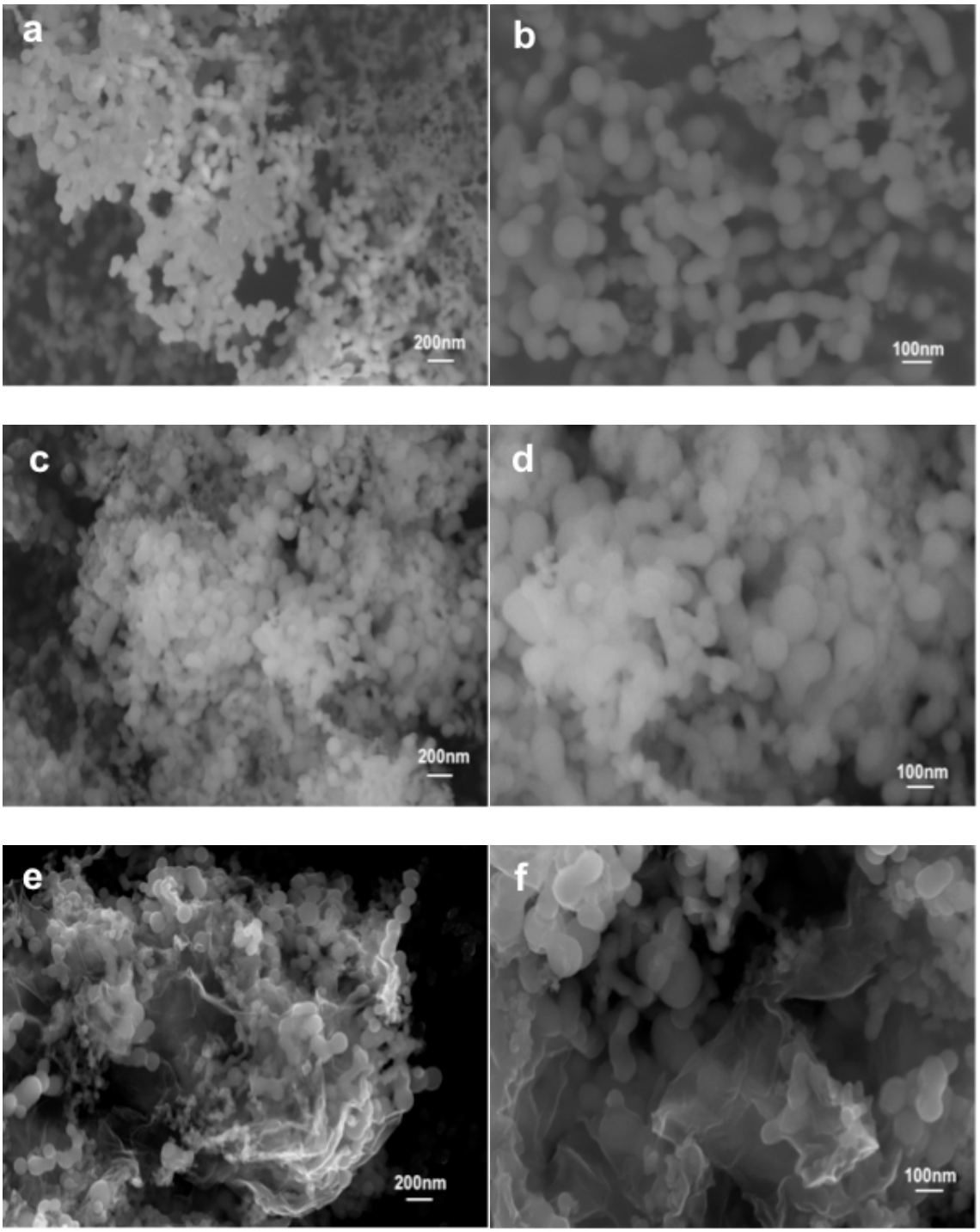

Figure 4.3: SEM images of (a)(b) nano-Si, (c)(d) n-Si/PANi, and (e)(f) n-Si/PANi/RGO at different magnifications

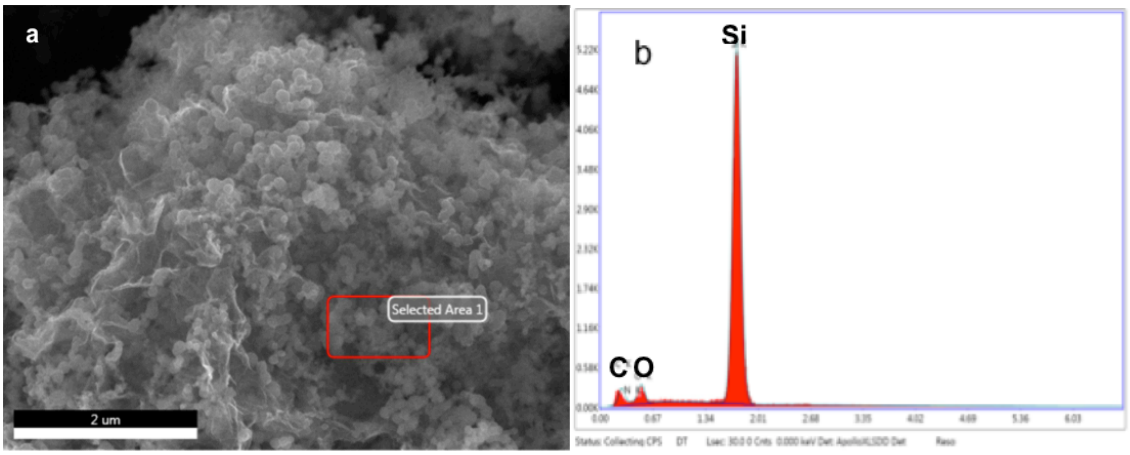

Figure 4.3 EDX result of nano-Si/PANi/RGO composite.

4.3 TEM images

TEM data of nano-Si, n-Si/PANi, and n-Si/PANi/RGO corroborate the SEM results. As seen in Figure 4.4 (a), the nano-Si particles have an interlinked spherical morphology with average particle size around 60 nm. The silicon particles in the n-Si/PANi composite (Figure 4.4 (b)) are interconnected through PANi "bridges". The same structure is observed in the n-Si/PANi/RGO composite (Figure 4.4 (c)) except that it is anchored on the RGO sheets. In this case, the RGO sheets form another network that further joints the nano-silicon particles and PANi matrix together. This structure may provide some interesting features for the electrochemical performance of the composite, namely, improved electrical conductivity of the composite in comparison to n-Si/PANi and deterrence of the aggregation of silicon nanoparticles, reducing the chances of particle pulverization upon repeated litigation/de-lithiation processes [115].

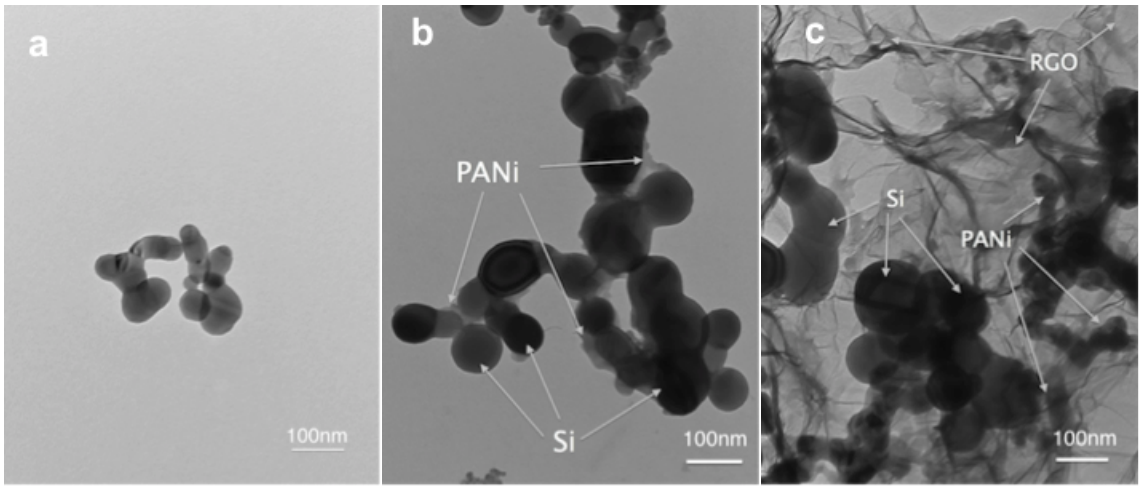

Figure 4.4: TEM images of (a) nano-Si, (b) n-Si/PANi and (c) n-Si/PANi/RGO composites.

4.4 TGA analysis

The Si content in n-Si/PANi and n-Si/PANi/RGO composites was determined by means of TGA analysis. Figure 4.5 shows that PANi begins to react with oxygen in air at low temperature and lost the majority of its mass in the range from 400 to 600 °C range while RGO starts to decompose rapidly in the range from 450 to 600 °C. Nearly all of their masses are lost at 600°C. On the contrary, silicon nanoparticles gain mass starting at temperatures above 600 °C indicating the formation of SiOx. Based on these observations and on the TGA profiles of the n-Si/PANi and n-Si/PANi/RGO composites, their Si content were determined as 85% and 68% respectively. These results are in close agreement whit the EDX analysis of n-Si/PANi/RGO (Supplemental Information).

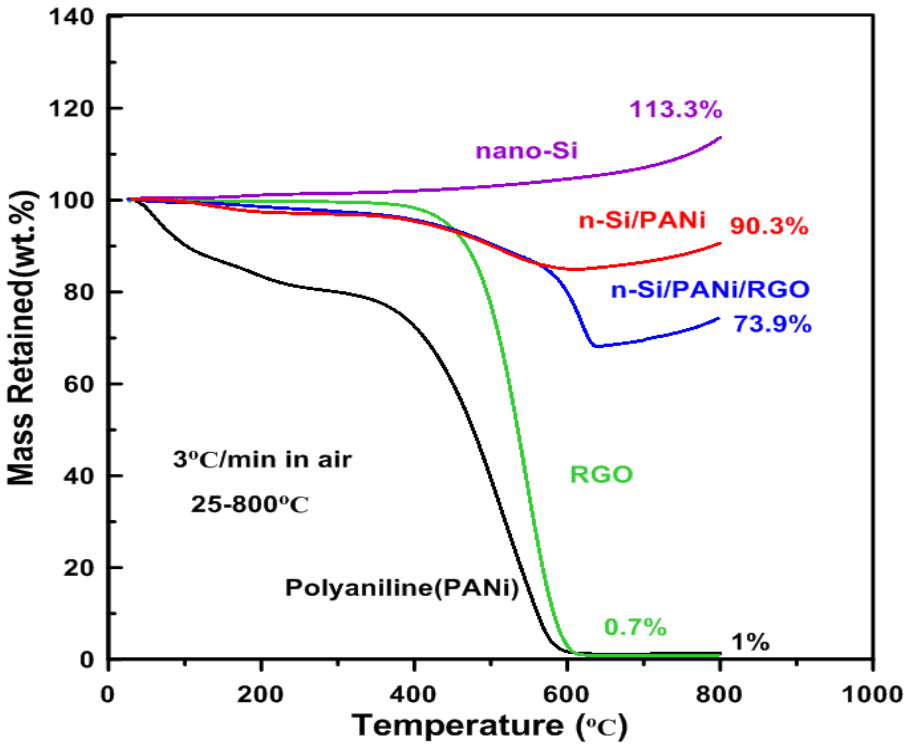

Figure 4.5: TGA results of nano-Si, n-Si/PANi, n-Si/PANi/RGO composites, reduced graphene oxide (RGO) and polyaniline (PANi) in air.

4.5 Electrochemical Performance

4.5.1 Cyclic voltammetry (CV) test

The cyclic voltammograms depicted in Figure 4.6 reveal that the three anode materials display similar CV profiles. The cathodic sweep of the CV curve shows one convoluted peak at 0.20 V attributed to the formation of Li–Si alloy phases. The anodic peak at 0.50 V is ascribed to reverse de-alloying of Li–Si. The increase in current intensity during the cycling is mainly because the active material is being activated during the test. No other peaks were detected in the potential range scanned, which indicates that the PANi is electrochemically inactive between 0.01–2.0V [24].

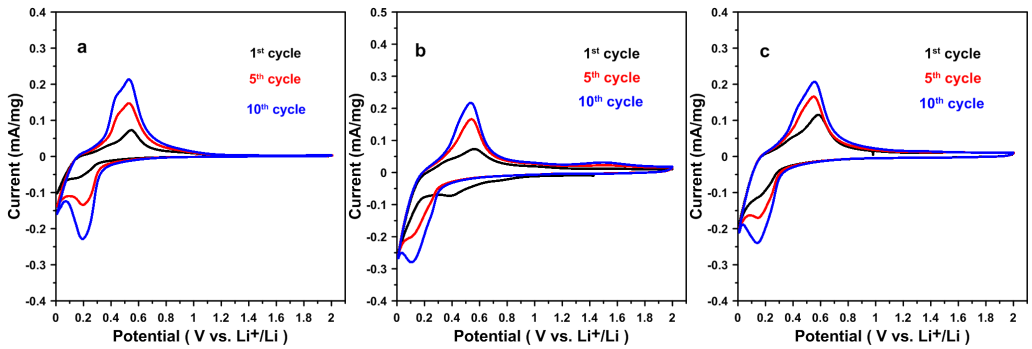

Figure 4.6: Cyclic voltammograms of (a) nano-Si (b) n-Si/PANi and (c) n-Si/PANi/RGO composites at constant scanning rate of 0.1mV/s.

4.5.2 Cycling performance test

Figure 4.7 shows the voltage profiles of nano-Si, n-Si/PANi and n-Si/PANi/RGO between 0.01 and 2.0 V vs. Li+/Li at constant current density of 200mA/g. The nano-Si anode (Figure 4.7 (a) and (b)) delivers initial specific capacity of 3286 mAh/g with a coulombic efficiency of 85.3%. However, the capacity sharply decreases to 1080 mAh/g after 30 cycles with a fading rate of about 2.2% per cycle. The slightly improved cyclability observed here is likely due to the higher content of CMC binder [24, 116-118]. An initial specific capacity of 3072 mAh/g and coulombic efficiency of 82.8% is observed for the n-Si/PANi anode, which shows a better capacity retention maintaining 1634 mAh/g after 30 cycles (1.6% cycling capacity fading rate). The n-Si/PANi/RGO anode shows better overall cycling performance (Figure 4.7 (e) and (f)) attaining an initial specific capacity of 3259 mAh/g with 83.5% coulombic efficiency. The capacity drops to 2000 mA/g after 30 cycles, equivalent to a fading rate of 1.3% per cycle. Table 4.2 shows the summary of the cycling performances. The n-Si/PANi/RGO composite displays a better overall performance with higher reversible capacity, better capacity retention, and stable coulombic efficiency.

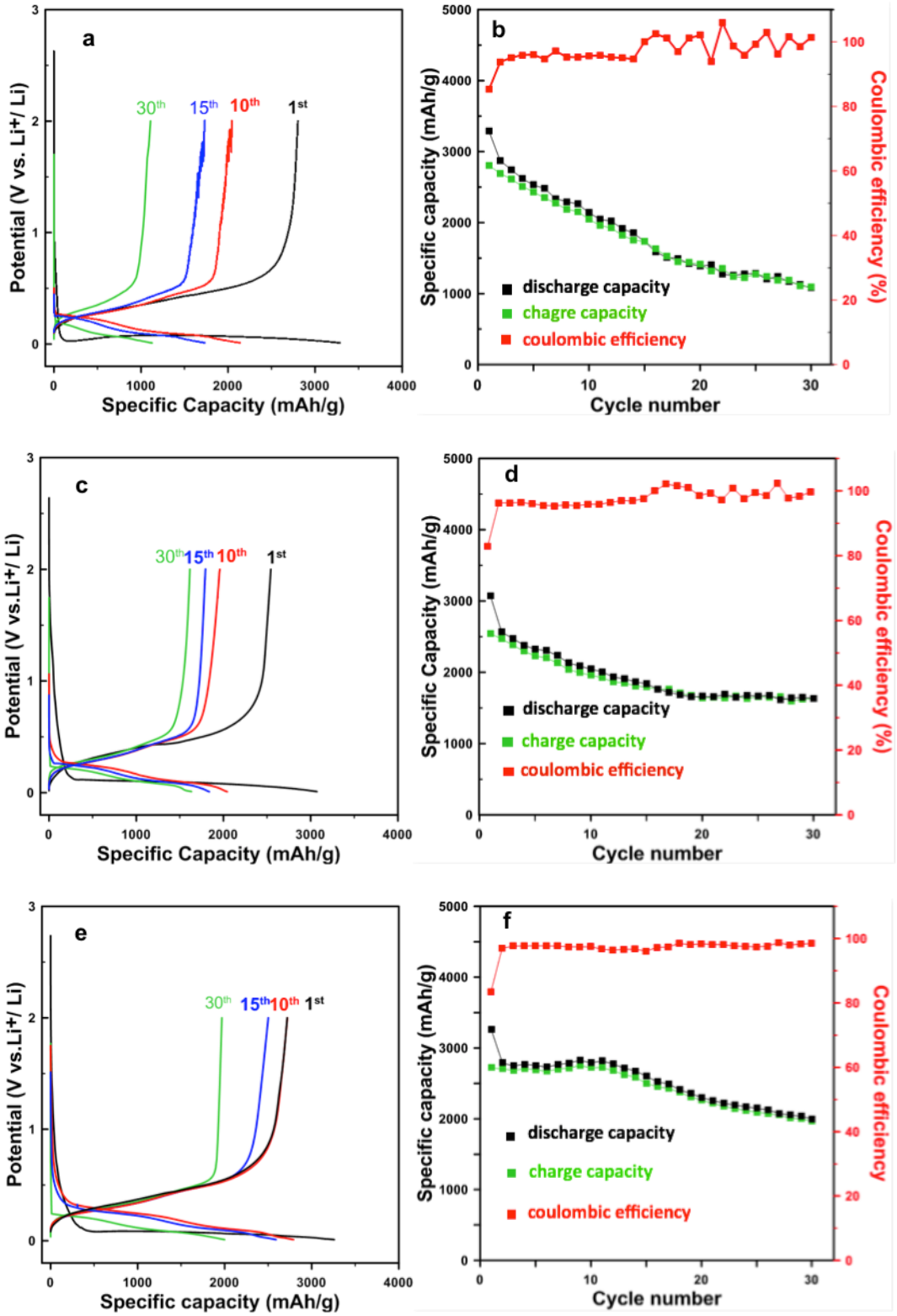

Figure 4.7: Voltage profile and cycling performance of (a) (b) nano-Si, (c)(d) n-Si/PANi and (e)(f) n-Si/PANi/RGO at constant current density of 200mA/g.

Table 4.2: Summary of cycling performance for nano-Si, n-Si/PANi and n-Si/PANi/RGO

Material	Initial capacity (mAh/g)	Capacity after 30 cycles (mAh/g)	Capacity fading rate				
			1-10 cycles	10-20 cycles	20-30 cycles	Overall	Per cycle (avg.)
nano-Si	3286	1080	35%	23%	9%	67%	2.2%
n-Si/PANi	3072	1634	34%	12%	1%	47%	1.6%
n-Si/PANi/RGO	3259	2000	14%	15%	9 %	38%	1.3%

4.5.3 Rate capability test

Rate capability tests were carried out in order to study the performances of all three materials under different current densities. The results, shown in Figure 4.8, reveal the superior performance of the n-Si/PANi and n-Si/PANi/RGO composites. When the current density increases to 500 mA/g the specific capacity of the n-Si/PANi/RGO drops to and roughly stabilizes at ~2200 mAh/g whereas the stable capacity for the n-Si/PANi composite and nano-Si are at 1500mAh/g and 1000mAh/g, respectively. Upon continued increase in current density the capacity of the nano-Si drops to ~500mAh/g but the n-Si/PANi/RGO and n-Si/PANi composites still maintain approximately 1300mAh/g and 800mAh/g reversible specific capacity. Nonetheless, under these conditions, all three materials perform poorly, mainly because the limited Li^+ ion transport rate and electrical conductivity could not satisfy the high rate operation. When the current density is reduced back to 200mAh/g, n-Si/PANi/RGO recovers 70.4% of its initial capacity whereas nano-Si and n-Si/PANi only realize 35.6% and 50.1% recovery, respectively. Furthermore, n-Si/PANi/RGO exhibits better rate capability than nano-Si or n-Si/PANi. The better rate capability and capacity recovery performance of n-Si/PANi/RGO is likely a result of its better electrical conductivity.

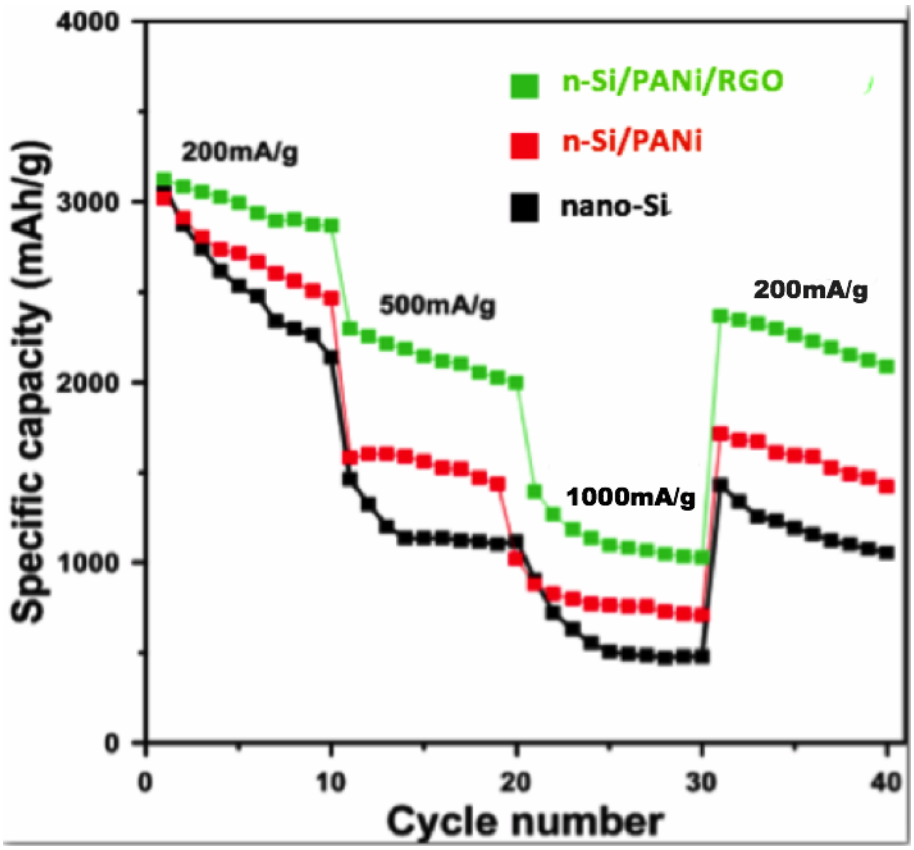

Figure 4.8: Rate performances for nano-Si, n-Si/PANi and n-Si/PANi/RGO composites.

4.5.4 AC impedence test

The unique nanostructure of the n-Si/PANi/RGO, confirmed by electron microscopy, affords good electrical connection and charge transport between silicon nanoparticles, PANi matrix and RGO sheets. This is corroborated by AC impedance measurements (Figure 4.9). The Nyquist plots of cells with nano-Si, n-Si/PANi and n-Si/PANi/RGO anodes prior cycling show a semicircle in the medium-frequency region, usually assigned to the charge-transfer resistance [43, 119]. The n-Si/PANi/RGO anode has faster charge transfer than the nano-Si and n-Si/PANi counterparts.

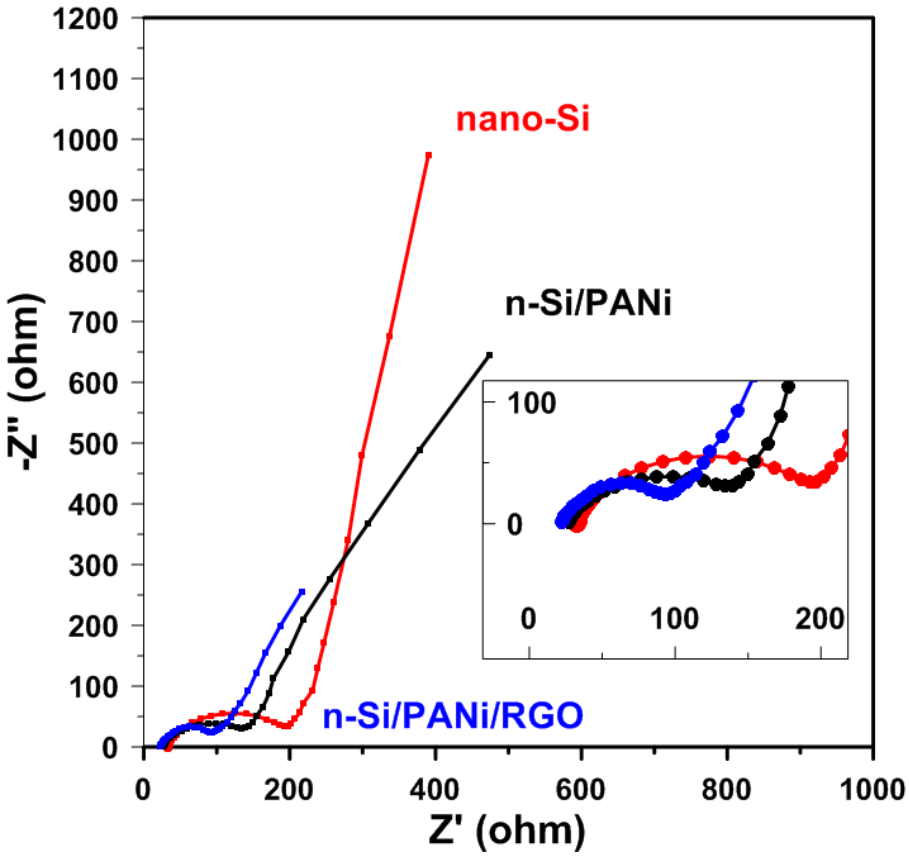

Figure 4.9: Nyquist plots for nano-Si, n-Si/PANi and n-Si/PANi/RGO composites.

In summary, n-Si/PANi/RGO composite was synthesized via a two-step process: preparation of n-Si/PANi composite by in-situ polymerization of polyaniline in DTAB aqueous solution followed by combination of the as-prepared n-Si/PANi composite with RGO. Electron microscopy analysis reveals the unique nano-architecture of the ternary composite, which comprises of well-dispersed silicon nanoparticles within polyaniline matrix that is further anchored on the surface of RGO sheets. CV tests, cycling tests, rate capability tests and AC impedence tests were carried out on n-Si/PANi, n-Si/PANi/RGO composites and nano-Si to study and compare electrochemical performance of these three anode materials.

The cyclic voltammetry tests reveal that nano-Si, n-Si/PANi and n-Si/PANi/RGO anode materials display similar CV profiles. The cathodic sweep of the CV curve shows one convoluted peak at 0.20 V attributed to the formation of Li–Si alloy phases. The anodic peak at 0.50 V is ascribed to

reverse de-alloying of Li–Si. No other peaks were detected in the potential range scanned, which indicates that the PANi is electrochemically inactive between 0.01–2.0V.

Rate capability test shows that nano-Si/PANi/RGO could deliver better rate capability and capacity recovery than either nano-Si or n-Si/PANi. The improved performance of the nano-arquitectured n-Si/PANi/RGO composite is attributed to its higher electrical conductivity and stabilization of the Si nanoparticles.

AC impedance tests of nano-Si, n-Si/PANi and n-Si/PANi/RGO anodes prior cycling real that the n-Si/PANi/RGO anode has faster charge transfer than the nano-Si and n-Si/PANi counterparts.

Chapter 5 Conclusions

5.1 Conclusions

In this work, nano-silicon/polyaniline/reduced graphene oxide composite was synthesized via a two-step process: in-situ polymerization of polyaniline (PANi) in the presence of nano-silicon followed by combination of the prepared n-Si/PANi binary composite with reduced graphene oxide (RGO) to form a n-Si/PANi/RGO composite. Scanning and transmission electron microscopy reveal the unique nano-architecture of the n-Si/PANi/RGO composite. Silicon nanoparticles are well dispersed within a PANi matrix which in turn is anchored to the surface of RGO sheets. The nano-Si particles, reduced graphene oxide sheets and polyaniline conductive matrix form a homogeneous nano-architectured composite in which nano-Si is well dispersed. This morphology should hinder agglomeration of the nanoparticles, thus preventing pulverization upon cycling, an increased capacity could be expected.

CV tests, cycling tests, rate capability tests and AC impedence tests were carried out on n-Si/PANi, n-Si/PANi/RGO composites and nano-Si to study and compare electrochemical performance of these three anode materials. Cycle performance tests show that nano-Si anode delivers initial specific capacity of 3286 mAh/g with a coulombic efficiency of 85.3%. However, the capacity sharply decreases to 1080 mAh/g after 30 cycles with a fading rate of about 2.2% per cycle. An initial specific capacity of 3072 mAh/g and coulombic efficiency of 82.8% is observed for the n-Si/PANi anode, which shows a better capacity retention maintaining 1634 mA/g after 30 cycles (1.6% cycling capacity fading rate). The n-Si/PANi/RGO anode shows better overall cycling performance attaining an initial specific capacity of 3259 mAh/g with 83.5% coulombic efficiency. The capacity drops to 2000 mA/g after 30 cycles, equivalent to a fading rate of 1.3% per cycle. The n-Si/PANi/RGO composite displays a better overall performance with higher reversible capacity, better capacity retention, and stable coulombic efficiency.

The cyclic voltammetry tests reveal that nano-Si, n-Si/PANi and n-Si/PANi/RGO anode materials display similar CV profiles. The cathodic sweep of the CV curve shows one convoluted peak at 0.20 V attributed to the formation of Li–Si alloy phases. The anodic peak at 0.50 V is ascribed to

reverse de-alloying of Li–Si. No other peaks were detected in the potential range scanned, which indicates that the PANi is electrochemically inactive between 0.01–2.0V.

Rate capability test shows that nano-Si/PANi/RGO could deliver better rate capability and capacity recovery than either nano-Si or n-Si/PANi. The improved performance of the nano-arquitectured n-Si/PANi/RGO composite is attributed to its higher electrical conductivity and stabilization of the Si nanoparticles.

AC impedance analysis reveal that the n-Si/PANi/RGO composite has higher electrical conductivity than the other two materials yielding better performance at high current densities.

The good rate performance, high initial specific capacity and stable coulombic efficiency of n-Si/PANi/RGO make it a promising anode material for high energy density lithium-ion batteries.

5.2 Suggestions for future work

Searching for long-lasting high energy density Lithium-Ion Batteries is a long-term goal. The research and development of anodes with high energy density and great cyclability needs to be done in order to achieve such goal.

Nano-Si/PANi/RGO composite as one of those promising anode candidates for designing high energy density Lithium-Ion Batteries system for different purposes shows great rate performance associated with high specific capacity and stable coulumbic efficiency. However, it also has an issue on cycling stability. To solve this problem, some future work should be done to fix such problem including following the aspects:

a) Change preparation procedure. For example, prepare nano-si/RGO composite by hydrolysis TEOS on the RGO sheets then reduce nano-SiO_2 to nano-Si. After that, in-situ polymerization of polyaniline could be carried out in the presence of nano-si at RGO sheets. The in-situ synthesis of nano-si directly on the RGO sheets make the bonding between nano-si and RGO strong which helps to stable the unique nanostructure.
b) Optimize the weight ratio of nano-si, polyaniline and reduced graphene oxide. The different weight ratio of nano-si, polyaniline and reduced graphene oxide in the nano-Si/PANi/RGO composite may show different effect on the electrochemical performance of nano-Si/PANi/RGO composite, more work should be done in this topic in order to get an optimization weight ratio to over come the cycling stability issue.

Also, more work should be invested into searching for high capacity and long-lasting cathode to improve the overall capacity of the battery since the energy density of the full Lithium-Ion Batteries system is not only determined by anode materials.

Last, methods for in-situ characterization of battery material need to be invented in order to study the electrochemical reactions, such as Li-metal/non-metal alloying, and oxidation/reduction. With the help of such techniques, we could also study the mechanical integrity of the nano-architectures and mechanism of SEI formation during repeated charge/discharge process.

References

[1] Denker, J. S. (2003). “Timescale for Depletion of Fossil Energy Resources." from http://www.av8n.com/physics/fossil-resources.htm - htoc1.

[2] J. M. Tarascon and M. Armand (2001). “Issues and challenges facing rechargeable lithium batteries.” Nature 414: 359

[3] Wanli Xu (2011). “Silicon nanowire anode for lithium-ion batteries: Fabrication, characterization and solid electrolyte interphase.” PHD Dissertation

[4] Yueping Yao (2008). “A study of electro materials for lithium-ion batteries.” PHD Dissertation

[5] Lide, D. R. (1990). “CRC Handbook of Chemistry and Physics”. Boca Raton Ann Arbor Boston, CRC Press

[6] A. Robinson (1974). “Lithium Primary Cells: Serendipitous Search for a New Laser Leads to an Advanced Battery Science.” 1984: 554

[7] E.S. Takeuchi, W.C, Thiebolt (1988). “The Reduction of Silver Vanadium Oxide in Lithium/Silver Vanadium Oxide Cells.” J. Electrochem. Soc. 135: 2691

[8] A. Crespi, C.Schmidt, J. Norton, K.Chen, P. J. Skarstad (2001). “Modeling and Characterization of the Resistance of Lithium/SVO Batteries for Implantable Cardioverter Defibrillators.” J. Electrochem.Soc. 148(1) A30-A37

[9] K.M. Abraham, D.M. Pasquariello, and F.J. Martin (1986). “Mixed Ether Electrolytes for Secondary Lithium Batteries with Improved Low Temperature Performance.” J. Electrochem Soc. 133: 661

[10] B.M.L.Rao, R.W. Francis, H.A. Christopher (1977). “Lithium-Aluminum Electrode.” J. Electrochem Soc. 124: 1490-1492

[11] P. Sanchez, C. Berlin, C.Crepyand A.De Guibert (1989). “Electrochemical studies of lithium-boron alloys in non-aqueous media — comparison with pure lithium.” J.appl. Electrochem. 19(3): 421-423

[12] United States Patent (1979), 4,302,518

[13] M. Zanini, S. Basu, J.E. Fischer (1978). "Alternate Synthesis & Reflectivity Spectrum of Stage 1 Lithium-Graphite Intercalation Compound." Carbon 16: 211-212

[14] M.M. Thackeray, W.I.F. David, P.G. Bruce, and J.B. Goodenough (1983). “Lithium insertion into manganese spinels.” Materials Research Bulletin 18(4): 461–472

[15] Padhi, A. K. (1997). “Phospho-olivines as positive-electrode materials for rechargeable lithium batteries." Electrochem. Society 144 (4): 1188–1194

[16] M. Armand, in: Materials for Advanced batteries, eds.D.W. Murphy, J. Broadhead and B.C.H. Steele (Plenum Press, New York, 1980): 145

[17] Teki, R., Datta, M. K., Krishnan, R., Parker, T. C., Lu, T.-M., Kumta, P. N. and Koratkar, N. (2009). "Nanostructured Silicon Anodes for Lithium Ion Rechargeable Batteries." Small 5: 2236–2242

[18] Z. X.Shu, R.S. Mcmillan,J.J. Murry,J (1993). "Electrochemical Intercalation of Lithium into Graphite." J. Electrochem Soc. 140: 922

[19] Mary L. Patterson, Anode Materials for Lithium Ion Batteries, Indiana University Battery Workshop, Nov 13 2009.

[20] J.O. Besenhard, J. Yang and M. Winter (1997). "Will advanced lithium-alloy anodes have a chance in lithium-ion batteries?" J. Power Sources 68: 87-90

[21] k.d. Kepler, John T. Vaughey, and M.M. Thackeray (1999). "$Li_xCu_6Sn_5$ $(0 < x < 13)$: An Intermetallic Insertion Electrode for Rechargeable Lithium Batteries." Electrochemical and solid-state letters 2: 307-309

[22] W. J. Zhang (2011). "A review of the electrochemical performance of alloy anodes for lithium-ion batteries." Journal of Power Sources 196: 13–24

[23] O. Mao, R. L. Turner, I. A. Courtney, B. D. Fredericksen, M. I. Buckett, L. J. Krause, and J. R. Dahn (1999). "Active/Inactive Nanocomposites as Anodes for Li-Ion Batteries." Electrochem. Solid State Lett, 2: 3-5

[24] Jie-Jian Cai, Peng-Jian Zuo, Xin-Qun Cheng, Yu-Hong Xu, Ge-Ping Yin (2010). "Nano-silicon/polyaniline composite for lithium storage." Electrochemistry Communications 12: 1572–1575

[25] Hui Wu, Yi Cui (2012). "Designing nanostructured Si anodes for high-energy lithium ion batteries." Nano Today 7: 414-429

[26] US Patent 5, 478,671 (1995)

[27] L. Yuan, Z.P. Guo, K. Konstantinov, H.K. Liu, S.X. Dou (2006). "Nano-structured spherical porous SnO_2 anodes for lithium-ion batteries." Journal of Power Sources 159: 345–348

[28] Ohzuku,T., A. Ueda, and N. Yamamoto (1995). "Zero-strain insertion material of Li $[Li_{1/3}Ti_{5/3}]$ O_4 for rechargeable lithium cells." Journal of the Electrochemical Society 142(5): 1431-1435.

[29] L. Kavan, M. Grätzel (2002). "Facile Synthesis of Nanocrystalline $Li_4Ti_5O_{12}$ (Spinel) Exhibiting Fast Li Insertion." Electrochem. Solid-State Lett. 5: A39-A42.

[30] Zhenguo Yang, Daiwon Choi, Sebastien Kerisit, Kevin M. Rosso, DonghaiWang, Jason Zhang, Gordon Graff, Jun Liu (2009). "Nanostructures and lithium electrochemical reactivity of

lithium titanites and titanium oxides: A review." Journal of Power Sources 192:588–598
[31] Chan, C. K., R. Ruffo, S. S. Hong and Y. Cui (2009). "Surface chemistry and morphology of the solid electrolyte interphase on silicon nanowire Lithium-Ion Batteries anodes." Journal of Power Sources 189(2): 1132-1140.
[32] Graetz, J., C. C. Ahn, R. Yazami and B. Fultz (2003). "Highly reversible lithium storage in nanostructured silicon." Electrochemical and Solid State Letters **6**(9): A194-A197
[33] Hong Guo, Hailei Zhao, Chaoli Yin, Weihua Qiu (2006). "A nanosized silicon thin film as high capacity anode material for Li-ion rechargeable batteries." Materials Science and Engineering B 131: 173–176
[34] Ji Heon Ryu, Jae Woo Kim, Yung-Eun Sung, and Seung M. O (2004). "Failure Modes of Silicon Powder Negative Electrode in Lithium Secondary Batteries." Electrochemical and Solid-State Letters, 7 (10): A306-A309
[35] Z. P. Guo, E. Milin, J. Z. Wang, J. Chen, and H. K. Liu (2005). "Silicon/Disordered Carbon Nanocomposites for Lithium-Ion Batteries Anodes." Journal of The Electrochemical Society, 152 (11): A2211-A2216
[36] Y. Zhang, X.G. Zhang, H.L. Zhang, Z.G. Zhao, F. Li, C. Liu, H.M. Cheng (2006). "Composite anode material of silicon/graphite/carbon nanotubes for Li-ion batteries." Electrochimica Acta 51: 4994–5000
[37] Lanyao Shen, Xianwei Guo, Xiangpeng Fang, Zhaoxiang Wang, Liquan Chen (2012). "Magnesiothermically reduced diatomaceous earth as a porous silicon anode material for lithium ion batteries." Journal of Power Sources 213: 229-232
[38] Nikolay Dimov, Satoshi Kugino, Masaki Yoshio (2003). "Carbon-coated silicon as anode material for lithium ion batteries: advantages and limitations." Electrochimica Acta 48: 1579-1587
[39] Yoshio, M., H. Y. Wang, K. Fukuda, T. Umeno, N. Dimov and Z. Ogumi (2002). "Carboncoated Si as a Lithium-Ion Batteries anode material." Journal of the Electrochemical Society 149(12): A1598-A1603
[40] M. Gulbinska, F. S. Galasso, S. L. Suib, S. Iaconetti, P. G. Russell and J. F. DiCarlo (2002). "Carbon Coated Silicon Powders As Anode Materials For Lithium Ion Batteries." Solid-State Ionics (MRS Fall Meeting), 756
[41] Lu Yue, Suqing Wang, Xinyue Zhao and Lingzhi Zhang (2012). "Nano-silicon composites using poly (3,4-ethylenedioxythiophene): poly (styrenesulfonate) as elastic polymer matrix and carbon source for Lithium-Ion Batteries anode." J. Mater. Chem, 22, 1094–1099
[42] Lee, J. H., W. J. Kim, J. Y. Kim, S. H. Lim and S. M. Lee (2008). "Spherical

silicon/graphite/carbon composites as anode material for lithium-ion batteries." Journal of Power Sources 176(1): 353-358.

[43] Hongfa Xiang, Kai Zhang, Ge Ji, Jim Yang Lee, Changji Zou, Xiaodong Chen, Jishan Wu (2011). "Graphene/nanosized silicon composites for lithium battery anodes with improved cycling stability." Carbon, 49: 1787–1796

[44] Xiaosi Zhou, Ya-Xia Yin, Li-Jun Wan and Yu-Guo Guo (2012). "Facile synthesis of silicon nanoparticles inserted into graphene sheets as improved anode materials for lithium-ion batteries." Chem. Commun., 48: 2198–2200

[45] Xingcheng Xiao, John S. Wang, Ping Liu, Anil K. Sachdev, Mark W. Verbrugge, Daad Haddad, Michael P. Balogh (2012). "Phase-separated siliconetin nanocomposites for high capacity negative electrodes in lithium ion batteries." Journal of Power Sources 214: 258-265

[46] J.M. Yan, H.Z. Huang, J. Zhang, Y. Yang (2008). "The study of Mg2Si/carbon composites as anode materials for lithium ion batteries." Journal of Power Sources 175: 547–552

[47] G.X. Wang, L. Sun, D.H. Bradhurst, S. Zhong, S.X. Dou, H.K. Liu (2000). "Nanocrystalline NiSi alloy as an anode material for lithium-ion batteries." Journal of Alloys and Compounds 306: 249–252

[48] Kasavajjula, U., C. Wang and A. J. Appleby (2007). "Nano- and bulk-silicon-based insertion anodes for lithium-ion secondary cells." Journal of Power Sources 163(2): 1003-1039.

[49] Jae-Myung Lee, Heechul Jung, Yoon Hwa, Hansu Kim, Dongmin Im, Seok-Gwang Doo, Hun-Joon Sohn (2010). "Improvement of electrochemical behavior of Sn_2Fe/C nanocomposite anode with Al_2O_3 addition for lithium-ion batteries." J. Power Sources, 195: 5044.

[50] Y. Liu, Z.Y.Wen, X.Y.Wang, X.L. Yang, A. Hirano, N. Imanishi, Y. Takeda (2009). "Improvement of cycling stability of Si anode by mechanochemcial reduction and carbon coating." Journal of Power Sources 189: 480–484

[51] I. S. Kim, P. N. Kumta and G. E. Blongren (2000). "New Silicon and Titanium Boride Nanocomposite Anodes for Li-Ion Batteries." Electrochem Solid-State Lett., 3, 493

[52] X.N. Zhang, G.L. Pan, G.R. Li, J.Q. Qu, X.P. Gao (2007). "Si–Si_3N_4 composites as anode materials for lithium ion batteries." Solid State Ionics, 178: 1107–1112

[53] Heon-Young Lee, Sung-Man Lee (2004). "Carbon-coated nano-Si dispersed oxides/graphite composites as anode material for lithium ion batteries." Electrochemistry Communications, 6: 465–469

[54] Wei-Jun Zhang (2011). "A review of the electrochemical performance of alloy anodes for lithium-ion batteries." Journal of Power Sources 196:13–24

[55] S.Y. Chew, Z.P. Guo, J.Z. Wang, J. Chen, P. Munroe, S.H. Ng, L. Zhao, H.K. Liu (2007).

"Novel nano-silicon/polypyrrole composites for lithium storage." Electrochemistry Communications, 9: 941–946

[56] Chen, L. B., X. H. Xie, J. Y. Xie, K. Wang and J. Yang (2006). "Binder effect on cycling performance of silicon/carbon composite anodes for lithium ion batteries." Journal of Applied Electrochemistry 36(10): 1099-1104.

[57] Kasavajjula, U., C. S. Wang and A. J. Appleby (2007). "Nano- and bulk-silicon-based insertion anodes for lithium-ion secondary cells." Journal of Power Sources, 163(2): 1003-1039.

[58] Lestriez, B., S. Bahri, I. Sandu, L. Roué and D. Guyomard (2007). "On the binding mechanism of CMC in Si negative electrodes for Li-ion batteries." Electrochemistry Communications, 9(12): 2801-2806.

[59] Ning Ding, Jing Xu, Yaxuan Yao, GerhardWegner, Ingo Lieberwirth, Chunhua Chen (2009). "Improvement of cyclability of Si as anode for Li-ion batteries." Journal of Power Sources, 192: 644–651

[60] Michel Ulldemolins, Frédéric Le Cras, Brigitte Pecquenard (2013). "Memory effect highlighting in silicon anodes for high energy density lithium-ion batteries." Electrochemistry Communications 27: 22–25

[61] Cui, L. F., Y. Yang, C. M. Hsu and Y. Cui (2009). "Carbon-Silicon Core-Shell Nanowires as High Capacity Electrode for Lithium Ion Batteries." Nano Letters, 9(9): 3370-3374.

[62] Magasinski, A., P. Dixon, B. Hertzberg, A. Kvit, J. Ayala and G. Yushin (2010). "High performance lithium-ion anodes using a hierarchical bottom-up approach." Nature Materal, 9(4): 353-358.

[63] Juchen Guo, Ann Sun, Chunsheng Wang (2010). "A porous silicon–carbon anode with high overall capacity on carbon fiber current collector." Electrochemistry Communications, 12: 981–984

[64] Candace K. Chan, Hailin Peng, Gao Liu, Kevin McIlwrath, Xiao Feng Zhang, Robert A. Huggins, Yi Cui (2008). "High performance lithium battery anodes using silicon nanowires." Nature Nanotechnology 3: 31 - 35

[65] Helmut, F., H. Hauke, O.W. Emmanuel, C. Jurgen, R. Oliver, W. Andreas and N. Gerold (2010). "Silicon Nanowires as Anode Material in Lithium-Ion Batteries." ECS Meeting Abstracts, 1003(1): 44.

[66] Peng, K., J. Jie, W. Zhang and S. T. Lee (2008). "Silicon nanowires for rechargeable Lithium-Ion Batteries anodes." Applied Physics Letters 93(3)

[67] Huixin Chen, Ying Xiao, Lin Wang, Yong Yang (2011). "Silicon nanowires coated with copper layer as anode materials for lithium-ion batteries." Journal of Power Sources, 196: 6657–

6662

[68] Jun Qua, Huaqing Li, John J. Henry Jr., Surendra K. Martha, Nancy J. Dudney, Hanbing Xu, Miaofang Chi, Michael J. Lance, Shannon M. Mahurin, Theodore M. Besmann, Sheng Dai (2012). "Self-aligned Cu–Si core–shell nanowire array as a high-performance anode for Li-ion batteries." Journal of Power Sources, 198: 312– 317

[69] Wei Chen, Nan Jiang, Zhongli Fan, Abirami Dhanabalan, Chunhui Chen, Yunjun Li, Mohshi Yang, Chunlei Wang (2012). "Facile synthesis of silicon films by photosintering as anode materials for lithium-ion batteries." Journal of Power Sources, 214: 21-27

[70] Peng, B., F. Y. Cheng, Z. L. Tao and J. Chen (2010). "Lithium transport at silicon thin film: Barrier for high-rate capability anode." Journal of Chemical Physics 133 (3)

[71] Sethuraman, V. A., M. J. Chon, M. Shimshak, V. Srinivasan and P. R. Guduru (2010). "In situ measurements of stress evolution in silicon thin films during electrochemical lithiation and delithiation." Journal of Power Sources, 195(15): 5062-5066.

[72] Sethuraman, V. A., V. Srinivasan, A. F. Bower and P. R. Guduru (2010). "In Situ Measurements of Stress-Potential Coupling in Lithiated Silicon." Journal of the Electrochemical Society, 157(11): A1253-A1261

[73] Christensen, J. (2010). "Modeling Diffusion-Induced Stress in Li-Ion Cells with Porous Electrodes." Journal of the Electrochemical Society, 157(3): A366-A380.

[74] Ohara, S., J. Suzuki, K. Sekine and T. Takamura (2004). "A thin film silicon anode for Li-ion batteries having a very large specific capacity and long cycle life." Journal of Power Sources, 136(2): 303-306.

[75] J. P. Maranchia, A. F. Heppb, A. G. Evansc, N. T. Nuhfera, P. N. Kumta (2006). "Interfacial properties of the a-Si/Cu: active-inactive thin film anode system for lithium-ion batteries." J. Electrochem. Soc. 153(6): A1246-A1253

[76] Madhuri Thakur, Mark Isaacson, Steven L. Sinsabaugh, Michael S. Wong, Sibani Lisa Biswal (2012). "Gold-coated porous silicon films as anodes for lithium ion batteries." Journal of Power Sources 205: 426– 432

[77] Y.Y. Tang, X.H. Xia, Y.X. Yu, S.J. Shi, J. Chen, Y.Q. Zhang, J.P. Tu (2013). "Cobalt nanomountain array supported silicon film anode for high-performance lithium ion batteries." Electrochimica Acta, 88: 664–670

[78] Y.Q. Zhang, X.H. Xia, X.L. Wang, Y.J. Mai, S.J. Shi, Y.Y. Tang, C.G. Gu, J.P. Tu (2012). "Three-dimensional porous nano-Ni supported silicon composite film for high-performance lithium-ion batteries." Journal of Power Sources 213: 106-111

[79] Heon-Cheol Shin, James A. Corno, James L. Gole, Meilin Liu (2005). "Porous silicon

negative electrodes for rechargeable lithium batteries." Journal of Power Sources, 139: 314–320
[80] Ying Zheng, Jun Yang, Jiulin Wang, Yanna NuLi (2007). "Nano-porous Si/C composites for anode material of lithium-ion batteries." Electrochimica Acta, 52: 5863–5867
[81] Ming-Shan Wang, Li-Zhen Fan, Mian Huang, Jinhong Li, Xuanhui Qu (2012). "Conversion of diatomite to porous Si/C composites as promising anode materials for lithium-ion batteries." Journal of Power Sources, 219: 29-35
[82] Taeseup Song, Jianliang Xia, Jin-Hyon Lee, Dong Hyun Lee, Moon-Seok Kwon, Jae Man Choi, Jian Wu, Seok Kwang Doo, Hyuk Chang, Won Il Park, Dong Sik Zang, Hansu Kim, Yonggang Huang, Keh-Chih Hwang, John A. Rogers, and Ungyu Paik (2010). "Arrays of Sealed Silicon Nanotubes As Anodes for Lithium Ion Batteries." Nano Lett., 10, 1710–1716
[83] Jaehwan Ha, Ungyu Paik (2012). "Hydrogen treated, cap-opened Si nanotubes array anode for high power lithium ion battery." Journal of Power Sources, in press, 1-6
[84] Hui Wu, Gerentt Chan, Jang Wook Choi, Ill Ryu, Yan Yao, Matthew T.McDowell, Seok Woo Lee, Ariel Jackson, Yuan Yang, Liangbing Hu and Yi Cui (2012). "Stable cycling of double-walled silicon nanotube battery anodes through solid–electrolyte interphase control." Nature Nanotechnology 7, 310–315
[85] Yan Yao, Matthew T. McDowell, Ill Ryu, Hui Wu, Nian Liu, Liangbing Hu, William D. Nix, and Yi Cui (2011). "Interconnected Silicon Hollow Nanospheres for Lithium-Ion Batteries Anodes with Long Cycle Life." Nano Letter, 11, 2949–2954
[86] Xiang-yang Zhou, Jing-jing Tang, Juan Yang, Jing Xie, Lu-lu Ma (2013). "Silicon@carbon hollow core–shell heterostructures novel anode materials for lithium ion batteries." Electrochimica Acta 87: 663– 668
[87] Nian Liu, Hui Wu, Matthew T. McDowell, Yan Yao, Chongmin Wang, and Yi Cui (2012). "A Yolk-Shell Design for Stabilized and Scalable Li-Ion Battery Alloy Anodes." Nano Letter, 12 (6): 3315–3321
[88] Hui Wu, Guangyuan Zheng, Nian Liu, Thomas J. Carney, Yuan Yang, and Yi Cui (2012). "Engineering Empty Space between Si Nanoparticles for Lithium-Ion Batteries Anodes." Nano Letter, 12, 904−909
[89] Perla B. Balbuena, a. Y. W. (2004). "Lithium-Ion Batteries: Solid-Electrolyte Interphase." Imperial College Press
[90] Scrosati, W. A. v. S. a. B. (2002). "Advances in Lithium-Ion Batteries." New York Kluwer Academic/Plenum Publisher
[91] Aurbach, D., B. Markovsky, I. Weissman, E. Levi and Y. Ein-Eli (1999). "On the correlation between surface chemistry and performance of graphite negative electrodes for Li ion batteries."

Electrochimica Acta, 45(1-2): 67-86.
[92] Chan, C. K., R. Ruffo, S. S. Hong and Y. Cui (2009). "Surface chemistry and morphology of the solid electrolyte interphase on silicon nanowire Lithium-Ion Batteries anodes." Journal of Power Sources, 189(2): 1132-1140.
[93] P. Verma, P. Maire, P. Novak (2010). "A review of the features and analyses of the solid electrolyte interphase in Li-ion batteries." Electrochim. Acta 55: 6332—6341
[94] R. Ruffo, S.S. Hong, C.K. Chan, R.A. Huggins, Y. Cui (2009). "Impedance Analysis of Silicon Nanowire Lithium Ion Battery Anodes." J. Phys. Chem. C 113: 11390—11398
[95] C.K. Chan, R. Ruffo, S.S. Hong, Y. Cui (2009). "Surface chemistry and morphology of the solid electrolyte interphase on silicon nanowire Lithium-Ion Batteries anodes." J. Power Sources 189:1132—1140
[96] Kong, F., R. Kostecki, G. Nadeau, X. Song, K. Zaghib, K. Kinoshita and F. McLarnon (2001). "In situ studies of SEI formation." Journal of Power Sources 97(8): 58-66
[97] Choi, N. S., K. H. Yew, H. Kim, S. S. Kim and W. U. Choi (2007). "Surface layer formed on silicon thin-film electrode in lithium bis(oxalato) borate-based electrolyte." Journal of Power Sources 172(1): 404-409
[98] Song, S. W. and S. W. Baek (2009). "Silane-Derived SEI Stabilization on Thin-Film Electrodes of Nanocrystalline Si for Lithium Batteries." Electrochemical and Solid State Letters 12(2): A23-A27
[99] Yen, Y. C., S. C. Chao, H. C. Wu and N. L. Wu (2009). "Study on Solid-Electrolyte-Interphase of Si and C-Coated Si Electrodes in Lithium Cells." Journal of the Electrochemical Society 156(2): A95-A102
[100] Flake, J. C., M. M. Rieger, G. M. Schmid and P. A. Kohl (1999). "Electrochemical etching of silicon in nonaqueous electrolytes containing hydrogen fluoride or fluoroborate." Journal of the Electrochemical Society 146(5): 1960-1965
[101] Kim, Y. L., Y. K. Sun and S. M. Lee (2008). "Enhanced electrochemical performance of siliconbased anode material by using current collector with modified surface morphology." Electrochimica Acta 53(13): 4500-4504.
[102] Huang, R., X. Fan, W. C. Shen and J. Zhu (2009). "Carbon-coated silicon nanowire array films for high-performance Lithium-Ion Batteries anodes." Applied Physics Letters, 95(13)
[103] Yu, Y., L. Gu, C. B. Zhu, S. Tsukimoto, P. A. van Aken and J. Maier (2009). "Reversible Storage of Lithium in Silver-Coated Three-Dimensional Macroporous Silicon." Advanced Materials 22(20): 2247
[104] Xiao, J., W. Xu, D. Y. Wang, D. W. Choi, W. Wang, X. L. Li, G. L. Graff, J. Liu and J. G.

Zhang (2010). “Stabilization of Silicon Anode for Li-Ion Batteries.” Journal of the Electrochemical Society, 157(10): A1047-A1051

[105] Choi, N. S., K. H. Yew, K. Y. Lee, M. Sung, H. Kim and S. S. Kim (2006). “Effect of fluoroethylene carbonate additive on interfacial properties of silicon thin-film electrode.” Journal of Power Sources, 161(2): 1254-1259

[106] Libao Chen, Ke Wang, Xiaohua Xie, Jingying Xie (2007). “Effect of vinylene carbonate (VC) as electrolyte additive on electrochemical performance of Si film anode for lithium ion batteries.” Journal of Power Sources, 174: 538–543

[107] Egerton, R. F. (2005). “Physical principle of electron microscopy: an introduction to TEM, SEM, and AEM.” New York, Springer.

[108] Stuart, B. H. (2004). “Infrared Spectroscopy: Fundamentals and Applications.” London John Wiley & Son Ltd.

[109] W, Redfern, J. P. (1963). “Thermogravimetric Analysis: A Review.” Analyst 88: 906-924.

[110] William S. Hummers Jr., Richard E. Offeman (1958). “Preparation of Graphitic Oxide.” J. Am. Chem. Soc., 80: 1339–1339

[111] M.N. Obrovac, L.J. Krause (2007). “Reversible Cycling of Crystalline Silicon Powder.” J. Electrochem. Soc. 154: A103

[112] M.S.P. Shaffer, X. Fan, and A.H. Windle (1998). “Dispersion and packing of carbon nanotubes.” Carbon, 36 (11): 1603

[113] S.X. Xing, H.W. Zheng, G.K. Zhao (2008). “Preparation of polyaniline nanofibers via a novel interfacial polymerization method.” Synth. Met. 158: 59–63 [16] T.Q. Wang, W.B. Zhong, X.T. Ning, Y.X. Wang, W.T. Yang, J. Colloid Interface Sci. 334 (2009) 108–112.

[114] T.Q. Wang, W.B. Zhong, X.T. Ning, Y.X. Wang, W.T. Yang (2009). “Facile synthesis of polyaniline “sunflowers” with arrays of oriented nanorods.” J. Colloid Interface Sci. 334: 108–112.

[115] Renlong Liang, Huaqiang Cao, Dong Qian, Jingxian Zhang, Meizhen Qu (2011). “Designed synthesis of SnO2-polyaniline-reduced graphene oxide nanocomposites as an anode material for lithium-ion batteries.” J. Mater. Chem., 21: 17654

[116] S.Y. Chew, Z.P. Guo, J.Z. Wang, J. Chen, P. Munroe, S.H. Ng, L. Zhao, H.K. Liu (2007). “Novel nano-silicon/polypyrrole composites for lithium storage.” Electrochem. Commun. 9: 941-946.

[117] Y.H. Xu, G.P. Yin, Y.L. Ma, P.J. Zuo, X.Q. Cheng (2010). "Nanosized core/shell silicon@carbon anode material for lithium ion batteries with polyvinylidene fluoride as carbon source." J. Mater. Chem. 20: 3216-3220.

[118] Chou SL, Wang JZ, Choucair M, Liu HK, Stride JA, Dou SX (2010). "Enhanced reversible lithium storage in a nanosize silicon/graphene composite." Electrochem Commun., 12: 303–306.

[119] Scrosati, B. (1995). Challenge of Portable Powder." Nature, 373: 557-558

[120] Gholam-Abbas Niazri, GianFranco Pistoia (2009). "Lithium ion batteries: Science and Technology." Springer, Michigan USA: 129-130.